Master's thesis

NTNU
Norwegian University of Science and Technology
Faculty of Natural Sciences
Department of Chemical Engineering

Stina Laugen

Selective Recovery of Lithium from Lithium-Ion Batteries (LIBs) of Electrical Vehicles (EVs)

Master's thesis in Chemical Engineering
Supervisor: Sulalit Bandyopadhyay
Co-supervisor: Christian Rosenkilde
June 2021

NTNU
Norwegian University of
Science and Technology

Stina Laugen

Selective Recovery of Lithium from Lithium-Ion Batteries (LIBs) of Electrical Vehicles (EVs)

Master's thesis in Chemical Engineering
Supervisor: Sulalit Bandyopadhyay
Co-supervisor: Christian Rosenkilde
June 2021

Norwegian University of Science and Technology
Faculty of Natural Sciences
Department of Chemical Engineering

NTNU
Norwegian University of
Science and Technology

Abstract

Lithium-ion batteries (LIBs) dominate in the electric vehicle (EV) market due to their excellent performance. The recent growth is primarily driven by the electrification of transportation. Despite a recession in overall sales due to the covid-19 pandemic, an increase of 137% from 2020-2021 exhibits a sensational success in the global sales of EVs. This growing global demand for electric vehicles increases the necessity for circularity in terms of recycling. Furthermore, it is predicted that the future market of LIBs will primarily be constrained by the supply of raw materials – especially in the power storage segment.

Europe is approaching a challenge with waste management as the first generation of LIBs is expected to reach their end of life in the very near future. To be ahead of time and be able to efficiently manage the expected volume of both waste and to effectively manage recycling requirements, an infrastructure needs to be established urgently.

The overall goal for the LIBRES project is to develop a pilot plant to treat the Norwegian volume of EOL LIBs by 2025. The goal must be in conjunction to criteria of cost efficiency and reduced environmental impacts. Employing a hydrometallurgical approach will redeem the requirements and furthermore encounter the goal of high recovery rates. This work aims to selectively recover lithium in the context of resource savings and meeting demands for the increasing EV market, as a part of the LIBRES project.

Selective lithium recovery from spent LIBs of EVs using oxalic acid and chemical precipitation was investigated. The black mass was dissolved by inorganic and organic acid. The leaching was followed by removal of impurities and selective Li recovery through precipitation.

The results demonstrate that sulfuric acid in the presence of a reducing agent aided the efficiency and provide efficiencies in the range of 83-100% for the different metals. Selective lithium dissolution was succeeded using oxalic acid, maximum efficiency of 63% was achieved with an s/l-ratio of 30 g/L and 53˚C. The use of organic acid generated an additional step to recover the remaining metals, and the subsequent inorganic acid leaching yielded lower efficiencies (-83%, -40%, and -16% for Ni, Co, and Mn, respectively) compared to the one of the initial black mass directly. Recovery of solid lithium in the form of Li_2CO_3 was insufficient, considering the 16% efficiency. However, treating anode and cathode together will contribute to the goal of increased automation. Additionally, it will decrease operational costs.

KEYWORDS: Electrical Vehicles, LIB, Recycling, Hydrometallurgy, Oxalic acid, Li recovery

Preface

This master thesis is carried out on the behalf of the research group of Environmental Engineering and Reactor Technology (EERT) at the Department of Chemical Engineering. The research work is conducted between January 2021 – June 2021.

I would like to express my gratitude to my internal supervisor Prof. Sulalit Bandyopadhyay, Department of Chemical Engineering, for valuable guidance and scientific supervision throughout the research period. He has a working capacity that I have never witnessed before, despite a hectic schedule, he was always helpful. I would also like to thank my external co-supervisor, Christian Rosenkilde, Hydro, for providing an industrial perspective and useful advice that greatly contributed to the work.

Moreover, I would like to thank my lab-partner Tryanti Melinda Sinambela for mental support and scientific discussions during the study. Jose Paulino Peris Sastre, I really appreciate all scientific advice regarding laboratory practice and for your contribution in making the study room a pleasant workplace. I would like to express profound my gratitude and indebtedness to Jack White for reviewing my thesis prior to submission.

Finally, my heartfelt thanks go to the closest friends and family for the love, encouragement, and meaningful conversations. This thesis would not have seen the light of day without the unconditional support from their presence.

I hereby declare that this is an independent piece of work performed in accordance with the exam regulations of the Norwegian University of Science and Technology.

Stina Laugen

Trondheim, 18.06.2021

Table of content

List of Figures

List of Tables

Abbreviations

EOL	End of life
EV	Electrical vehicle
H_2O_2	Hydrogen peroxide
H_2SO_4	Sulfuric acid
ICDD	The international Centre for Diffraction Data
LIB	Lithium-ion battery
MP-AES	Microwave Plasma Atomic Emission Spectrometer
Na_2CO_3	Sodium carbonate
NaOH	Sodium hydroxide
Na_2S	Sodium sulphide
NMC	Nickel manganese cobalt
$C_2H_2O_4$	Oxalic acid
XRD	X-Ray Diffraction
XRF	X-Ray Fluorescence

Thesis overview

Section 1 provides a synopsis - gives an insight into lithium-ion batteries, the state-of-the-art in the market of electrical vehicles, and incentives for recycling, along with the present situation and associated challenges.

In Section 2, the groundwork for the experiment is outlined. Chemical reagents, procedures and instrumentation used for qualitative and quantitative analysis is provided.

Section 3 is the analysis of the earlier segment and an associated discussion. The route of selective lithium recovery is thoroughly examined.

Section 4 provides a conclusion to the main discoveries of the study.

Suggestions for future work, including guidance to the enhancement of selective lithium recovery, are presented in **section 5.**

1. Introduction

Lithium-ion batteries (LIBs) dominate in the electric vehicle (EV) market due to their excellent performance, high energy density, cycle stability and lifetime [1, 2]. LIBs are very diverse with regards to the various applications they can be utilized for [3]. The recent growth is primarily driven by the electrification of transportation. Moreover, they are predicted to take an increasing role in stationary energy storage, like for wind and solar systems and they are emerging – combined with solar generation cells - as micro-storage power systems at the residential and small commercial level [1].

The exponential growth in demand and thus production capacity, leads to lower costs [1]. Additionally, they are more eco-friendly compared to other battery types, as they do not contain Pb and Cd [2]. Although the general design of LIBs (Figure 1.1) is fabricated from similar materials, there is a wide diversity in cell chemistry [4].

1.1 Lithium-Ion Battery Components and Cell Types

The battery cell is made up of two electrodes, a separator, electrolyte, and casings (Figure 1.1). Aluminium, steel, or plastic usually compose the outer casing/shell. A positive and negative electrode corresponds to the cathode and anode, in discharging mode, respectively. The anode is made of copper foil coated with graphite, while the cathode is an aluminium foil coated with metal oxides. The LIBs are usually referenced according to the cathode active material (CAM), with the most common ones being LCO ($LiCoO_2$), NMC-111 ($LiNi_{0.33}Mn_{0.33}Co_{0.33}O_2$), NMC-811, NMC-532 and LMO ($LiMn_2O_4$).

An electrically insulating membrane serves as a (ion-)permeable separator between the electrodes and prevents short-circuiting. The separator is soaked in an electrolyte of organic carbonates and a conductive lithium-salt, allowing the battery to operate on high voltages. During the discharge process lithium ions are transported by the electrolyte, from the graphite through the diffusive membrane and are inserted in the metal oxide structure (Figure 1.1) [1].

The various configurations of CAM determine energy density, stability, cost and power output of the battery. Especially the NMC cathode has gained interest lately, due to its structural stability, discharge capacity and cyclic performance [1, 4]. In general, enhanced qualities/features, extended driving range and governmental incentives are the main reasons for recent growth [1].

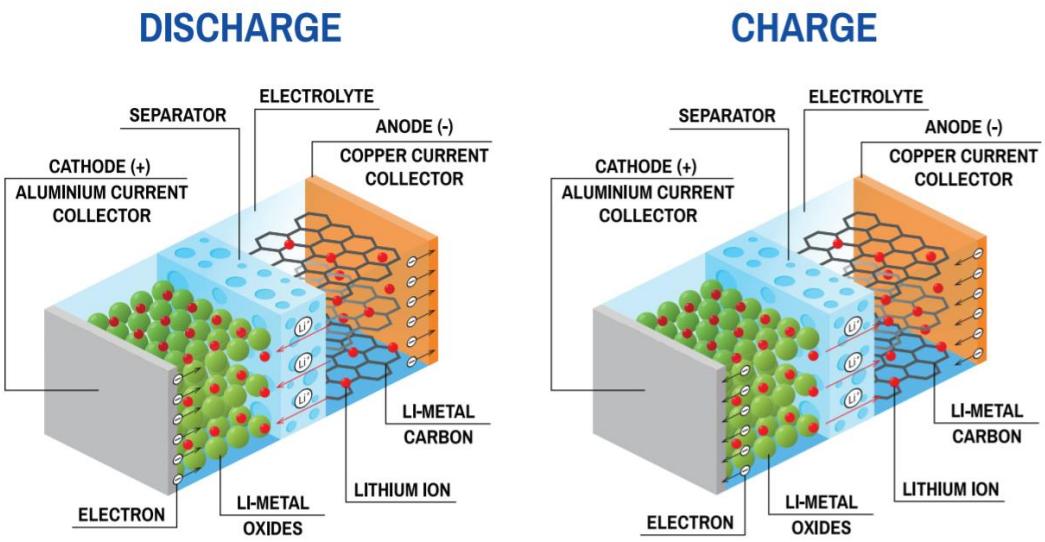

Figure 1.1. Major components and mechanism for LIBs [5].

1.2 Todays and Future EV market

The global EV sale has seen exponential growth over the past decade (Figure 1.2a), and the future outlook is solely positive one [1, 3]. Despite a sole recession due to the covid-19 pandemic, 2020 became a very successful year for EV sales in Europe with an increase of 137% from the previous year. Tax relief initiatives and increasingly convenient charging infrastructure are some of the main governmental policies that act as incentives for EV acquisitions [1].

The growing demand of electric vehicles and the preference for LIBs increases the necessity for circularity [3]. With the continuous industrial focus to enhance the electrochemical properties of the LIBs, follows a huge development in cell chemistries. Although improved performance is attempted by means of varying material composition, the batteries are still made up of the same matter [6], this is an important factor in the establishment of a reverse value chain i.e., recycling of valuable and scarce materials that can be put back into the production of new batteries, with respect to time [3].

When the battery has been removed from its original application permanently, it is referred to as an end-of-life (EOL) battery [3]. A recycling chain relies on the volume of EOL batteries. However, this quantity is not consistent with the number of new batteries being produced. To put it into perspective: back in 2019 an estimate of 47.8 GWh (175 tonnes) reached end-of-life, whereas 218 GWh (1 000 000 tonnes) were put on the market (Figure 1.2a). This reflects both the instant growth rate of manufacture and their potential lifetime [3].

Steady improvements result in enhanced properties such as cyclic stability and thus extended lifetime. Additionally, the cold climate of Europe will decelerate the degradation due to reduced aging rate of LIBs at lower temperatures [7]. The consequence is a slow growth in the volume of batteries reaching EOL. Along with this, factors such as frequency of use, deviation in user behaviour and possibilities for reuse makes it difficult to predict the annual volume of LIBs accessible for recycling. Accordingly, the uncertainty makes it more difficult/challenging for recyclers to obtain economics of scale [3].

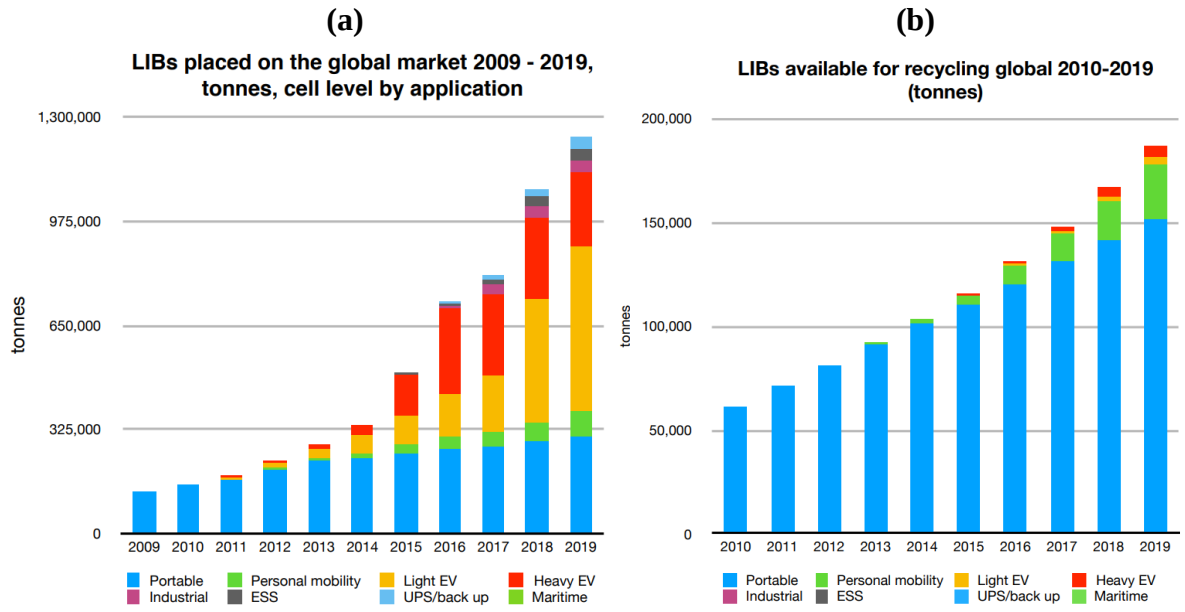

Figure 1.2. Tonnes of LIB placed on the (a) marked and (b) ready for recycling, respectively [3].

Although China has a high volume of EOL LIBs and a well-established recycling chain, the development of a proper recycling loop in Europe is paramount to the leading EV uptake. Europe [8]. The expected high volume of EOL LIBs in Europe in the coming years, will allow for the establishment of an efficient infrastructure [3].

1.3 Incentives for Battery Recycling

Although there are uncertainties related to the 8–10-year lifespan of LIBs, the constant growth imposes demand for an appropriate infrastructure, by means of LIB waste management and recovery of valuable metals. Currently, environmental issues are related to landfills and raw material extraction [1].

Recovery of scarce and precious metals are essential to preserve resources. Approximately 60% of the cobalt worldwide is extracted from mines in the Democratic Republic of Congo. Furthermore, cumulative lithium demand in China may exceed the country's reserves by the year of 2028. The uneven geographic distribution of resources poses economic strains [1].

Along with resource savings, recycling of LIBs and their components will lead to energy savings and environmental preservation. Especially the extraction, transportation and processing of Ni, Co, Li and Al all requires high amounts of power and cause emissions of harmful gases. Although some of the metals is not considerably valuable, recycling will save up to 95% of the total energy required from their virgin extraction [1].

The current situation is dominated by disposal to municipal landfills, in non-restricted regions. These landfills impose gradual deterioration to the environment when water is exposed to the waste and toxic metals leach out into the soil. Nonetheless, legislation can mitigate such issues and thereby drive the establishment of LIB recycling infrastructure [1, 9].

1.4 Current Situation and Challenges

The growth in electric transportation leads to increased cell manufacturing capacity, intermediary material production and raw material extraction. It is predicted that the future (2030 and onwards) market will be constrained by supply of raw materials [3, 10]. The first generation of LIBs implemented around 2015 are likely to reach end of their feasible practicality in the near future. To be ahead of time and be able to efficiently manage the coming waste concerns it is essential a framework is to be installed and provide a more imperishable solution.

Today, most facilities focus on Co recovery due to the economic gains. However, this trend is likely to shift as the market (gradually) substitute the LCO with (the mixed-metal) NMC cathode [1]. Moreover, the lack of a standardized battery design and fast evolving chemistry makes it challenging to establish a uniform recycling route to fit the whole range of batteries. However, a sufficient separation and high recovery rates can be obtained by using a combination of the different recycling methods, namely pyrometallurgy, hydrometallurgy and direct recycling [1]. Below (Table 1.1) is presented an overview of existing facilities in Europe and their routes of recycling [10, 11].

Table 1.1. A selection of LIB recycling plants in Europe and respective technologies [12].

Company	Technology	Main elements recovered
Umicore	Pyrometallurgy + Hydrometallurgy	Co, Ni, Cu, Fe, $CoCl_2$
Akkuser	Physical separation	Co, Cu, Fe
Duesenfeld	Hydrometallurgy	$CoSO_4$, $NiSO_4$, $MnSO_4$, Li_2CO_3, graphite
Accurec Recycling GmbH	Pyrometallurgy + Hydrometallurgy	Li_2CO_3, Co-alloy
EDI (Sarpi Veolia)	Hydrometallurgy	Cu, Al, Ni, Co, Mn, alloys, Li_2CO_3
SNAM SAS	Pyrometallurgy + Hydrometallurgy	Ni, Co, Fe
Valdi (Eramet)	Pyrometallurgy	Al_2O_3, Ni, Mn alloy
Volkswagen		
Glencore	Pyrometallurgy	Co–Ni–Fe alloy, Cu, Al, Fe
Nickelhütte Aue GmbH	Pyrometallurgy + Hydrometallurgy	Co, Ni, Mn

As can be seen from the already existing recycling plants (Table 1.1), the use of pyrometallurgical routes is abundant. Although the process has a high capacity, the heat treatment requires major energy consumption, causes hazardous emissions, and amounts of lithium are lost in the slag. Despite the present availability and lower cost of Li, it is not of significance yet, but the increasing demand of LIBs is expecting to pose a constraint in the raw material in the middle of this century, around 2050 (Section 1.3) [1].

Another challenge is related to the low volume of EOL batteries (Figure 1.2), which makes it difficult for recyclers to acquire economies of scale. For the recycling process to be efficient in terms of economics, there has to be a sufficient volume of EOL batteries. The possibility of repurposing and reuse in other applications after serving its intended purpose (in EVs), makes the market more complex and dynamic, thus even harder to predict [3].

From the numerous challenges, it seems like the overall goal is to reduce environmental impacts by means of lowering energy consumption and emission of harmful gases. Employing a hydrometallurgical approach will redeem most of the requirements and furthermore meet the goal of high recovery rates [1, 11].

1.5 Investigating Previous Research

As mentioned in the previous section, the increasing demand for LIBs imposes the need to establish a sufficient infrastructure. The various options with EOL batteries are reuse, reconditioning, or recycling (Figure 1.3). The recycling route (3) is made up of three paths, namely pyrometallurgy, hydrometallurgy, and direct recycling, a combination is often used [2, 9]. General methods used for metal recovery in a hydrometallurgical approach, with emphasis on lithium, will be covered in this section.

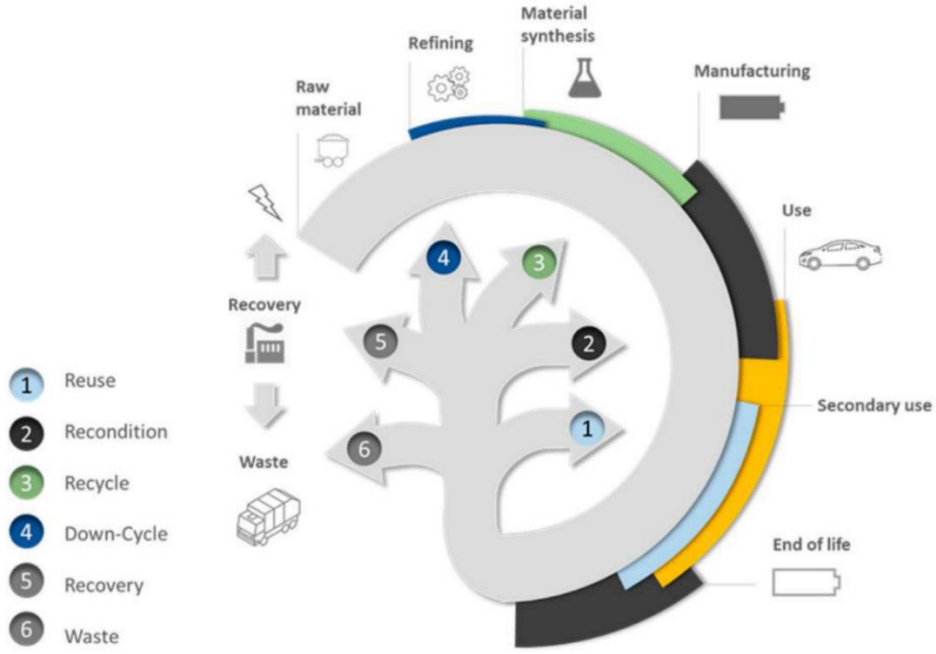

Figure 1.3. Flowchart of LIB circularity chain [9].

The recycling process is made up of several steps. First, the batteries are deactivated and dismantled to the cell level. After disassembly, follows crushing and sorting. High-temperature treatment can be used in this stage (i.e., pyrometallurgical processing), or the materials can be reused directly (i.e., direct recycling). After physical treatment follows a chemical route, usually including leaching, solvent extraction, and chemical precipitation, to recover the metal values (the hydrometallurgical part comprises the chemical processing) (Figure 1.4) [1, 13]. A greener recycling process has attracted more attention recently, in particular the elimination of heat treatment (i.e., entirely hydrometallurgical) [14].

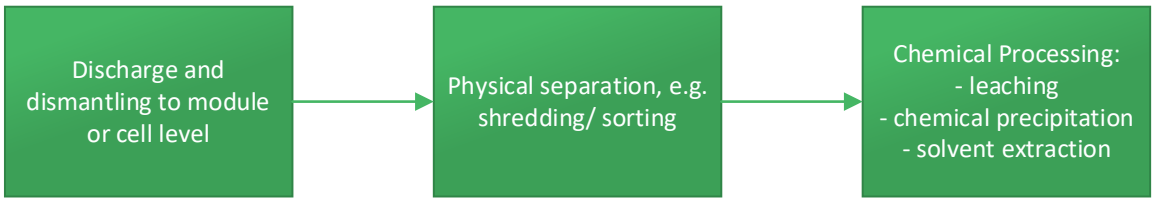

Figure 1.4. LIB recycling value chain [13].

Metal dissolution is extensively used in the metal industry. Inorganic and organic acids are employed to dissolve the metal ions into the solution (i.e., leaching). Sulfuric acid (H_2SO_4), nitric acid (HNO_3), and hydrochloric acid (HCl) are commonly used acids of the inorganic class. Although the inorganic acids provide high leaching efficiencies, they do adverse environmental impacts due to generation harmful gases such as SOx, Cl2 and NOx. For this reason, replacing it with an organic acid may reduce the environmental footprint and make the process more sustainable [15]. Of organic acids, oxalic acid ($H_2C_2O_4$), citric acid ($C_6H_8O_7$) and formic acid (CH_2O_2) have been used [2, 14].

The dissolution efficiency depends upon solid/liquid-ratio (pulp density), the concentration of leaching media, stirring rate, temperature, and leaching time. From previous research, it is demonstrated that increased temperature, acid concentration, and reaction time, along with a low s/l-ratio, will enhance the leaching efficiency [16-18].

Inorganic acid is often utilized in the presence of a reducing agent, such as hydrogen peroxide (H_2O_2), to increase the leaching efficiency. It reduces the metals to their divalent state (e.g., Co(III) to Co(II)), which enhances the solubility in the acidic solution [2, 15, 19]. Sulfuric acid dissolution of $N_1M_1C_1$ cathode material by addition of H_2O_2, can be explained by the reaction equation below [20]:

$$6LiNi_{0.33}Mn_{0.33}Co_{0.33}O_2 + 9H_2SO + H_2O_2 \rightleftharpoons$$

$$2MnSO_4 + 2NiSO_4 + 2CoSO_4 + 2LiSO_4 + 10H_2O + 2O_2 \quad (1)$$

In regard to oxalic acid leaching, the addition of H_2O_2 was found to be insignificant. In the presence of excess oxalic acid, the use of H_2O_2 only showed a slight increase in leaching efficiency, this may be due to its better ability to reduce metals [15]. Oxalic acid is known for its excellent properties as a ligand for metal ions [22]. For the separation of metals (Li, Ni, Mn, and Co) from spent LIBs, oxalic acid serves its purpose both as a dissolution, reducing, and precipitation agent [23]. The dissolution process of an $N_1M_1C_1$ type of cathode using oxalic acid can be described by the following reaction equilibrium [18]:

$$4H_2C_2O_4 + 2LiNi_{0.33}Mn_{0.33}Co_{0.33}O_2 \rightleftharpoons$$
$$Li_2C_2O_4 + 2(Ni_{0.33}Mn_{0.33}Co_{0.33})C_2O_4 + 4H_2O + 2CO_2 \quad (2)$$

Whereas lithium is dissolved into the solution, metals Ni, Co, and Mn of higher oxidation states are reduced and form metal oxalates which precipitates [18]. Table 1.2 outlines some research results from recovery processes proposed for LIB batteries. According to the table, lithium is easily leached out from spent LIB waste. The recovery of Ni, Mn, and Co through inorganic acid leaching, is emphasised in the last part of the table (Table 1.2) recovery.

Table 1.2. Summary of related research results for spent LIBs using inorganic and organic acid, with respect to lithium recovery.

Factors

Leaching agent	s/L ratio (g/L)	Temp. (˚C)	Time (hr)	Stirring	Metal recovery	Reference
0.6 M Oxalic acid	20	70	2	-	84% Li (NMC)	[18]
1 M Oxalic acid	10	95	12	-	95.4% Li (NMC)	[16]
1 M Oxalic acid	50	80	2	300	95% Li (LCO)	[21]
3 M oxalic acid	50	80	1.5	300	99% Li (LCO)	[17]

4 M Sulfuric acid + 30wt.% H_2O_2	50	70-80	2-3	-	≈ 100% LI, NI, MN, AND CO (NMC, LCO, LMO)	[2]
1 M Sulfuric acid	50	95	4	500	94.3% Li, 96.3% Ni, 50.2% Mn, and 66.2% Co (mixed)	[24]
2 M Sulfuric acid + 7.5wt.% H_2O_2	50	25	2	-	95.3% Li, 92.3% Ni, 92.1% Mn, and 91.7% Co (NMC)	[20]

The leachate composition is complex, and metals recovery is complicated. Various methods have been employed to recover metal ions from the leach liquor, chemical precipitation is widely used. The method is efficient in terms of the simple experimental setup and low operation costs. Chemical precipitation is a phenomenon occurring from supersaturated conditions [25]. Supersaturation is determined from solubility product (Ksp), temperature, concentration, ionic activity, and solution chemistry [26].

Commonly used precipitants are NaOH, NH_4OH, and Na_2CO_3. When the precipitation agents are added to the solution they dissolve and the resulting anions may combine with the metal ions to form hydroxides and carbonates [2, 27]. The soluble metals can be recovered as insoluble metal hydroxides according to the equation below [25]:

$$M^{2+} + 2(OH)^{-} \leftrightarrow M(OH)_2 \downarrow \quad (3)$$

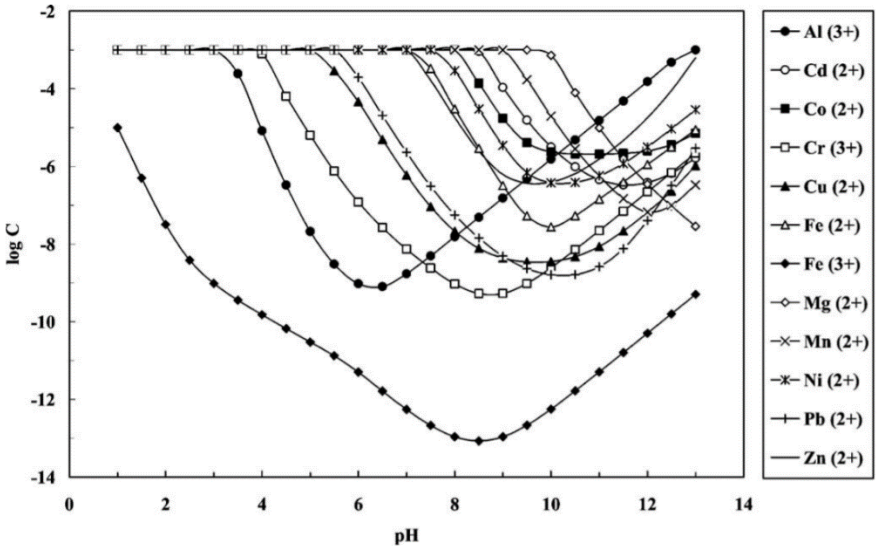

Figure 1.5. Solubility of metal hydroxides [25].

As seen from the solubility diagram above (Figure 1.5) and in literature, all the metals (Ni^{2+}, Mn^{2+}, and Co^{2+}) can be precipitated at a pH > 10. Although for Al^{3+}, Fe^{3+}, and Cu^{2+}, the solubility is increasing at a pH greater than 4 [25, 28].

As previously mentioned, carbonates can also be utilized for the precipitation of metals. The reaction of sodium carbonate with lithium oxalate is illustrated in the equation below [14, 18, 25]:

$$Na_2CO_3 + Li_2C_2O_4 \leftrightarrow Li_2CO_3 + Na_2C_2O_4 \quad (4)$$

Although carbonates can be used in precipitation, they do have higher pKs values and are accordingly more soluble [25, 29]. For the sake of Li_2CO_3, which is a basic salt, a lower pH will increase the solubility (due to the formation of HCO_3^- at lower pH values). Thus, a basic pH is desired to achieve supersaturation consequently precipitation [30]. Furthermore, the solubility of Li_2CO_3 decreases with increasing temperature. Zhang et al. managed to recover 81% of lithium as Li_2CO_3 using saturated Na_2CO_3 at 90˚C, the initial lithium concentration was 10 g/L [18]. Furthermore, 71 % recovery was obtained at an equilibrium pH of 10 at 50˚C (initial concentration of 20 g/L, 300 rpm for 1 hour) [30]. The solubility of selected inorganic compounds at different temperatures is provided in the table below (Table 1.3).

Table 1.3. Solubility of inorganic compounds in aqueous solution [29].

Aqueous solubility of inorganic compounds (g/100ml)				
Compound	25˚C	60˚C	80˚C	90˚C
LiOH	11.1	12.7	14.2	15.1
Li_2CO_3	1.28	0.99	0.85	0.78
$Li_2C_2O_4$	5.87	-	-	-
Na_2CO_3	23.5	31.7	31.3	30.9
$Na_2C_2O_4$	3.48	4.71	5.41	5.75
$Al_2(C_2O_4)\cdot H_2O$	Insoluble	-	-	-
$CoC_2O_4\cdot 2H_2O$	Insoluble	-	-	-
$CuC_2O_4\cdot 0.5H_2O$	Insoluble	-	-	-
$MnC_2O_4\cdot 2H_2O$	Insoluble	-	-	-
$NiC_2O_4\cdot 2H_2O$	Insoluble	-	-	-

By employing a hydrometallurgical route using the above-mentioned methods, the selective recovery of lithium in the form of lithium carbonate from EOL LIBs can be improved. Increasing the lithium recycling will contribute to the expected raw material constraints. The aim of this work is presented in the following section.

1.6 Aim and Scope of the Work

LIBRES (Lithium-ion Battery Recycling) is a Hydro owned project and a collaboration between several companies/ institutions, both commercial and research & development (R&D) organizations. Among others, Batteriretur AS, Glencore Nikkelverk AS, Elkem and NTNU. Batteriretur AS and NTNU are commercial and R&D partners, respectively. The project is also supported by Norsk Forskningsråd (NFR) [31].

The overall goal for the LIBRES project is to develop and commercialize a pilot plant large enough to handle the Norwegian volume of EOL LIBs by 2025. This goal must be in conjunction with cost efficiency, high recovery rates, and reduced environmental impacts. For the reason of constraints in raw material supply in the coming years, the emphasis on Li-recovery is highlighted. Furthermore, an automated process for deactivation and disassembly is desired [31].

This work aims to selectively recover lithium in the context of resource savings and meeting demands for the increasing EV market. The report will cover hydrometallurgical recycling strategies to recover materials from mixed-metal (NMC) LIB electrodes. Incentives for the choice of a hydrometallurgical process route are the insinuated lower environmental footprint and energy consumption (compared to pyrometallurgical) [1].

Spent, pre-treated LIBs of the prismatic cell type are supplied by Norsk Hydro ASA. After external mechanical pre-treatment, follows the dissolution of electrode material (black mass) through inorganic and organic acid leaching. The acidic leachate contains metal ions (Ni^{2+}, Mn^{2+}, Co^{2+}, Li^{2+}, Cu^{2+}, Al^{3+} and Fe^{3+}), which are recovered through subsequent precipitation steps. In this thesis work, the selective recovery of Li from spent LIBs of EVs by the use of oxalic acid and chemical precipitation is investigated, see the flowchart below (Figure 1.6).

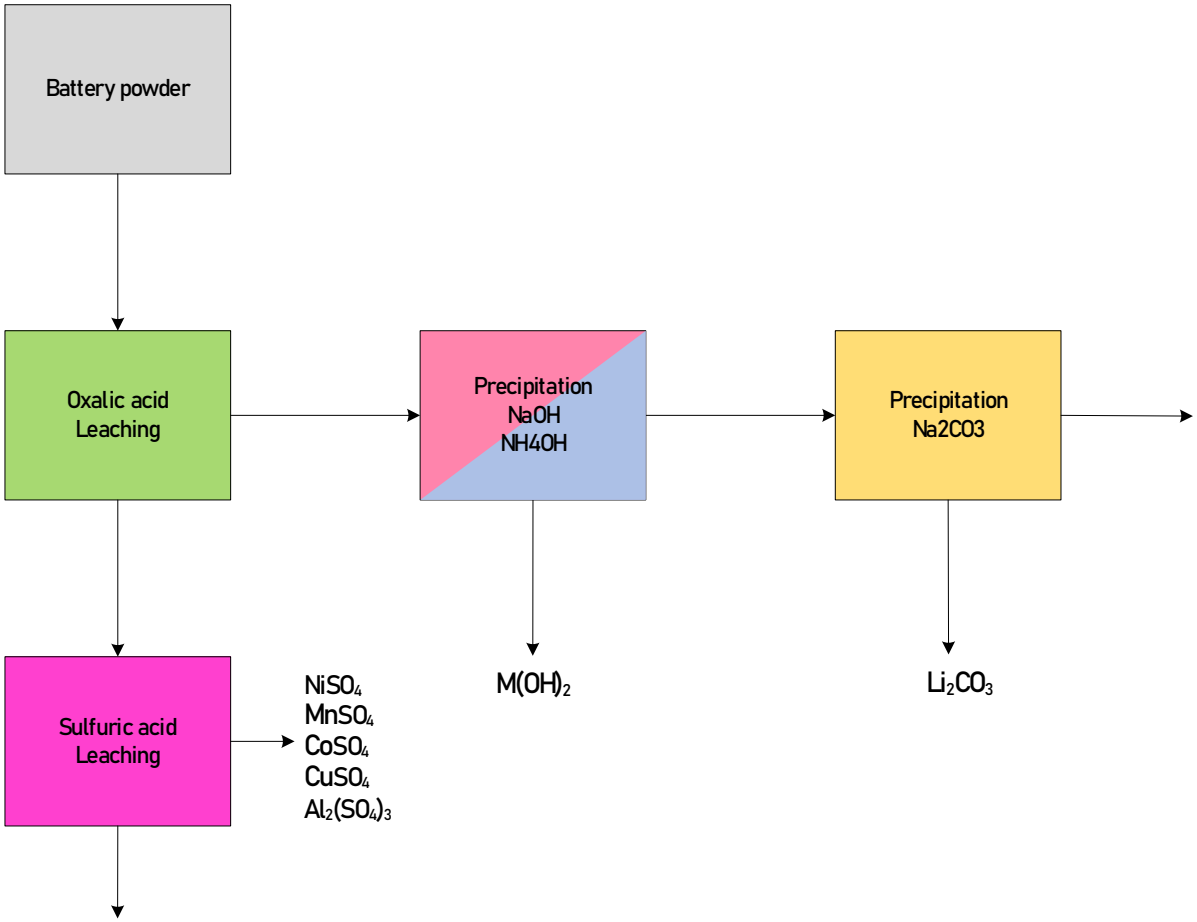

Figure 1.6. Overall flowsheet of experimental work. The colours represent the dye of solutions and are used in diagrams throughout the results and discussion to ease the reading.

2. Experimental

In this section, chemical reagents and experimental procedures are presented. Chemicals and analytical instruments are listed in the two first subsections, while the following sections provide experimental set-ups and procedures. Associated risk assessment for all experimental work is outlined and can be found in NTNUs risk register (ID: 40088).

The experimental part can be presented by the block flow diagram above (Figure 1.6). Apart from what is shown in this diagram, which is the route of selective lithium dissolution, an initial inorganic acid leaching was performed. The path of lithium recovery starts with an organic dissolution of the black mass to selectively leach out the lithium, followed by subsequent inorganic leaching to dissolve the remaining cathode material. Precipitation from the Li-rich solution by using NaOH and NH_4OH intends for impurity removal, while the last step has the purpose of selective lithium recovery through crystallization.

2.1. Chemical Reagents

Spent, pre-treated LIBs of the prismatic cell type were supplied by Norsk Hydro ASA. The initial pre-treatment done by Hydro is presented in table 2.1, and the resulting fine fraction (< 0.25 mm), the black mass, is utilized in this work. Compositional analysis of the black mass is performed by IME at RWTH Aachen (Table 2.2). For digestion of black mass, a mixture (3:1) of hydrochloric acid (HCl, 37% in purity) nitric acid (HNO_3, 70% in purity) made up an aqua regia solution. Sulfuric acid (H_2SO_4, 95% in purity) and oxalic acid ($C_2H_2O_4$, 98% in purity) were used as leaching agents. In addition to sulfuric acid, hydrogen peroxide (H_2O_2, 30 wt.%) served as a reductant. In the precipitation experiments, sodium hydroxide (NaOH, pellets for analysis), ammonium hydroxide (NH_4OH, 25% ammonia), and sodium carbonate (Na_2CO_3, ≥99% in purity) were used as precipitation agents. ICP Multi-element standard solution IV (1000 mg/L Ag, Al, B, Ba, Bi, Ca, Cd, Co, Cr, Cu, Fe, Ga, In, K, Li, Mg, Mn, Na, Ni, Pb, Sr, Tl, Zn) from Certipur® was used for the preparation of calibration standards prior to MP-AES analysis. All solutions were prepared with distilled water (DI) and all dilutions before analysis with ultrapure water (MQ). All chemicals are provided from Sigma Aldrich.

Table 2.1: Pre-treatment of spent LIBs performed by Hydro [13].

	Pre-treatment
Levels	Methodology
1	Discharge to 0 volt
2	Shredding in an inert atmosphere (argon or nitrogen).
3	Evaporation at negative pressure (100˚C and 0.1 bar)
4	Sieving, air separation, magnetic/ density/ Eddy current. The black mass is the < 250µm from the sieving.

Table 2.2. ICP-OES analysis of initial black mass performed by RWTH Aachen University. Elements C, F P, O, and S make up the remaining fraction and are excluded.

Electrode Composition (wt.%)						
Fe	Cu	Ni	Co	Li	Mn	Al
0.088	1.47	13.3	12.5	5.04	10.3	0.82

2.2. Metal Quantification and Characterization

To determine the composition/phases of solid samples (black mass, filter residues, and precipitates), a characterization by an X-ray Diffractometer (XRD, Bruker D8 A25 DaVinci) was conducted. The analysis was performed in the range of 10-80˚, with a step size of 0.013˚ and 0.66 sec step time, in total 2 hrs, for crystalline samples. For low crystallinity samples, the step size and step time were set to 0.050˚ and 3.7, respectively, resulting in a total measurement time of 1.5 h pr. sample.

Furthermore, the black mass was characterized using Wavelength Dispersive X-ray fluorescence (WD-XRF, Rigaku Supermini200). Particle morphology was examined using Scanning Electron Microscopy (SEM, FEI Apreo) at an accelerating voltage of 20 kV and a beam current of 0.4 nA.

Metal ions in solution were detected and quantified using Microwave Plasma Atomic Emission Spectrometer (MP-AES), which has high sensitivity and low detection limits [32]. External calibration curves were constructed by the MP-AES associated software from calibration standards (1-10 mg/L) (Appendix C). Standard solutions of 1-10 mg/L were prepared from dilution of a multi-metal 1000 mg/L stock solution. Solid samples were digested by the use of the Speedwave® Xpert Microwave Digestion System or dissolved manually prior to MP-AES analysis.

2.3. Digestion of Solid Samples

Digestion of solids was performed to determine the mass of metals in solid samples. For the digestion of powder, an aqua regia solution of HCl and HNO_3 (volumetric ratio of 4:1, respectively) was used. Digestion was done prior to metal detection using MP-AES, both with the initial black mass, filter cake residues and precipitates.

Approximately 0.08g of solid sample was weighed out in a beaker and 8mL of aqua regia (s/l-ratio of ~10g/L) was added and left to react for 2 hours in room temperature. The suspension was filtered and collected for analysis. The filtrate was diluted x1000 before MP-AES analysis. An illustration is shown in Figure 2.1.

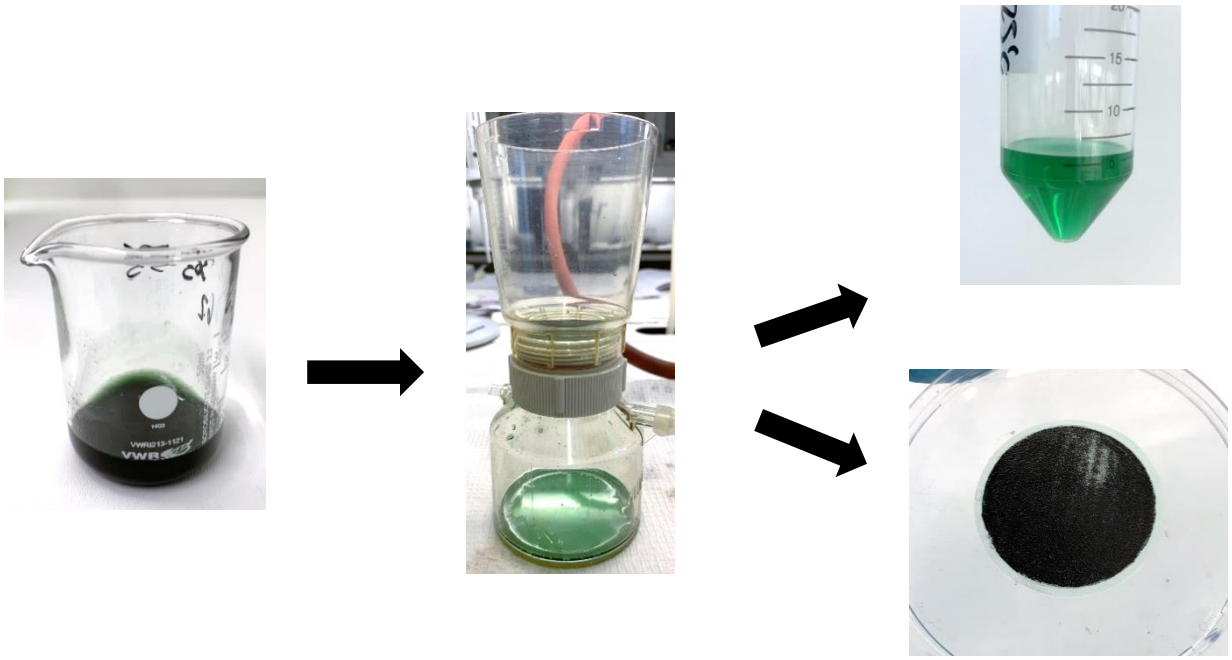

Figure 2.1. Illustration of aqua-regia digestion and subsequent vacuum filtration

2.4. Inorganic Acid Leaching

Initial leaching was performed to discover the most efficient way to leach out nickel, manganese, and cobalt, in terms of s/l-ratio and the presence of a reducing agent at 80˚C. Moreover, the efficiencies were compared those of organic acid leaching.

Inorganic acid was used to leach out metals from the spent LIB material. The temperature during experiments was controlled by means of an external heating circulator (Julabo SE-12) connected to the reactor. A condenser was attached to minimize the loss from evaporation, and a magnetic stirrer provided agitation.

Briefly, 7.5 g of black mass was added to a reactor with sulfuric acid (2M) in solid-liquid ratios ranging from 30-110 g/L (the volume of acid was adjusted accordingly). The temperature was set to 80˚C, stirring rate of 550 rpm and it was left to react for 1 hour. The same experiments were repeated with an H_2SO_4 solution containing 3.75 % H_2O_2, a complete overview is presented in table 2.3. Leaching set-up is adapted from previous work and depicted in figure 2.2 [33].

Table 2.3. Reaction conditions in inorganic leaching experiments. The naming X-X-X, indicate s/l-ratio and volume% of H2O2 (e.g., "sulfuric acid – 30g/l – 0 vol% H_2O_2").

	Factors	
No.	S:L (g/L)	H_2O_2 (vol%)
S-30-0	30	0
S-50-0	50	0
S-70-0	70	0
S-90-0	90	0
S-110-0	110	0
S-30-3.75	30	3.75
S-50-3.75	50	3.75
S-70-3.75	70	3.75
S-90-3.75	90	3.75
S-110-3.75	110	3.75

After leaching, the residue was filtered, and the leachate was collected in bottles for subsequent precipitation experiments. 1mL of the filtrate was diluted x1000 and analysed with MP-AES to determine the content of metals (Li, Co, Ni, Mn, Cu, Al, and Fe).

Figure 2.2. Leaching set-up. 250 mL glass reactor connected to heating circulator and condenser.

2.5. Organic Acid Leaching

The software JMP was used for the design of experiments (DOE), namely the feature "Definitive Screening Design". Given a range of continuous factors, in particular temperature (25-80˚C) and solid-liquid ratios (30g/L to 110g/L), and the setting "No blocks required" as a design option, it created a randomized list of 13 experiments (Table 2.4) to predicted how the factors affected the response (i.e., lithium concentration). When the resulting solution (leachate) was analysed and all data collected, JMP allowed you to visualize the results through statistical models such that one could see a pattern of responses, identify the dependent variables, and thus optimize the result (i.e., maximise Li concentration).

Oxalic acid was utilized for selective lithium dissolution of the black mass. The temperature during experiments was controlled though an external heating circulator (Julabo SE-12) connected to the reactor. A condenser was attached to minimize the loss from evaporation, and a magnetic stirrer provided agitation (Figure 2.2).

Firstly, a diluted oxalic acid solution (1M) was added to a 250 mL reactor. The reaction was temperature controlled by means of a heating circulator and a glass condenser was connected to minimize evaporation. ≈ 7.5 g of black mass were added to solutions in solid/liquid ratios of 30, 70, and 110 g/L. The corresponding volumes of oxalic acid were 0.25, 0.107, and 0.068 L, respectively. The temperature varied from 25˚C to 80˚C in the different experiments. All trials were carried out for 1 hr at a stirring rate of 550 rpm.

Table 2.4. Reaction conditions and levels of experiment generated from JMP DOE.

	Factors	
Levels	T (˚C)	S:L (g/L)
O-25-110.1	25	110
O-25-70	25	70
O-25-110.2	25	110
O-25-30.1	25	30
O-25-30.2	25	30
O-53-30	52.5	30
O-53-110	52.5	110
O-53-70	52.5	70
O-80-30.1	80	30
O-80-30.2	80	30
O-80-110.1	80	110
O-80-110.2	80	110
O-80-70	80	70

After leaching, the residue was filtered and collected in bottles for subsequent experiments. 1mL of the filtrate was diluted x1000 and analysed with MP-AES to detect the concentration of metals (Li, Co, Ni, Mn, Cu, Al, and Fe). The remaining powder (filter cake) was leached a second time using sulfuric acid for the purpose to dissolve the remaining metals.

2.5.1. Subsequent Dissolution of Solid Residues by Sulfuric Acid

As the industry continuously aims to enhance electrochemical properties, Ni-rich CAMs are to be expected in the future [6]. The conditions from 2.4. yielding the greatest mass of Ni (2M H_2SO_4, 3.75% H_2O_2, 110g/L, and 80˚C) was therefore chosen for the second leaching step. The leaching set-up (Figure 2.2) and the procedure are identical to the one described in section 2.4. Leaching efficiency is calculated from the following equation:

$$L\% = m_0/m_1 \cdot 100\% \quad (5)$$

2.6. Precipitation of Impurity Metals

To precipitate lithium from the leach liquor, the impurity metals (Ni, Mn, Co, Cu, and Al) had to be removed first. Ni, Mn, and Co are not usually considered impurities, but as this thesis focus on Li, it was desired to remove them. Moreover, the oxalic acid was used to selectively leach out Li, so the other metals were present in small quantities.

Cu, Al, Ni, Mn, and Co were removed from the leach solution by the addition of sodium hydroxide and ammonium hydroxide. The solution was heated to 60˚C at 300 rpm. The alkaline was thereafter added to the leach solution until the pH reached a value ≈10. The solution was left to react for 2 hours. The solution pH was measured using a pH meter (Mettler Toledo SevenEasy S20). A stagewise setup is presented below (Figure 2.3).

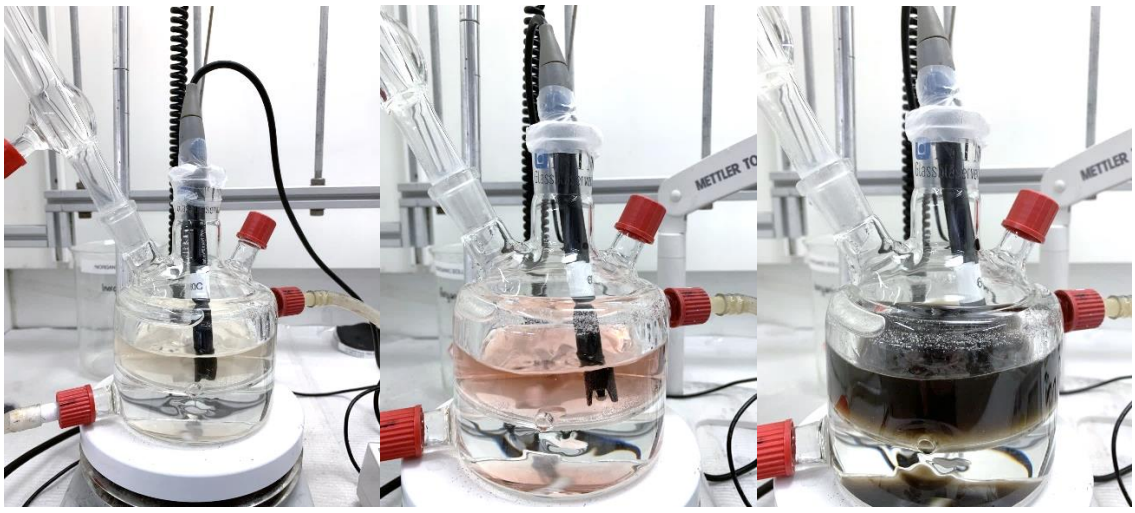

Figure 2.3. Precipitation of metal hydroxides by addition of NaOH, showing (a) no addition, (b) directly after addition and (c) at the end of precipitation.

After precipitation, the residue was filtered and collected in bottles for the subsequent Li precipitation. 1mL of the filtrate was diluted x1000 and analysed with MP-AES to detect the concentration of metals (Li, Co, Ni, Mn, Cu, Al and Fe). The precipitate was dissolved and analysed with MP-AES.

2.7. Selective Precipitation of Lithium

In order to precipitate the lithium, which was obtained from the previous precipitation experiment, another precipitation agent was applied. Li was precipitated from the supernatant solutions of section 2.6 by the addition of excess Na_2CO_3 (Figure 2.4) The precipitation agent was added in molar ratios of 1.5:1 (Na_2CO_3:Li^{2+}) [30]. The concentration of Li in the supernatant prior to the precipitation experiment was detected and calculated using MP-AES. The solution pH was monitored using a pH meter (Mettler Toledo SevenEasy S20).

Figure 2.4. Precipitation of lithium carbonate by addition of Na_2CO_3, showing (a) no addition, (b) directly after addition and (c) at the end of precipitation.

The crystallized solids were separated from the solution by vacuum filtration. The presence of metals in the filtrate was detected using MP-AES, and the precipitate obtained was characterized via XRD. All samples analysed with MP-AES were diluted x1000 prior to analysis. Precipitation efficiency is calculated from the following equation:

$$P\% = \frac{m_1 - m_2}{m_1} \cdot 100\% \quad (6)$$

Where m_0 and m_1 represent the mass of metal in leachate and supernatant, respectively.

2.8. Microwave digestion of Precipitates

The digestion of solid samples with the help of a microwave digestion system was performed in accordance with the digestion procedure provided by the supplier [34, 35]. 0.08g of precipitate was weighed out in weighing cups (accessories for speedwave microwave digestion) and transferred to the digestion vessels. The vessels were added 10 mL of HCl, mixed cautiously, and left 10 minutes for pre-reaction in the fume hood. Thereafter, the vessels were sealed and closed. A suitable digestion program (Table 1.1) was adjusted carefully and applied [35]. After the end of the program, the vessels were left to cool down before the samples were transferred to centrifuge tubes and diluted to 25 mL. 1000x dilution of the 25 mL sample was done before MP-AES analysis. The procedure is explained in the Berghof Speedwave instruction manual [35]. The initial powder and filtered suspension can be seen in figure 2.5.

Table 2.5. Application Note of solid sample digestion from Berghof [35].

Temperature program

Step	T (˚C)	p (bar)	Ramp (min)	Hold (min)	Power (%)
1	200	35	10	30	90
2	50	25	1	10	0

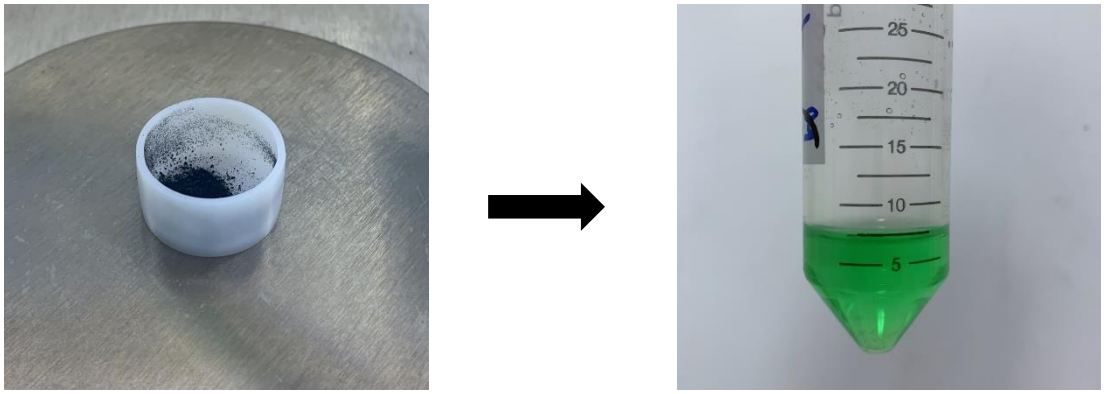

Figure 2.5 Metal hydroxide precipitate before and after digestion.

3. Results and Discussion

In this section, results obtained from the previous section (Section 2) will be presented, and the subsections will follow the same chronology as the associated flow chart (Figure 1.6). The composition of initial black mass, dissolution efficiencies, and presence of metals in solid samples will be discussed.

Throughout the R&D section (Section 3), concentration in terms of g/L is not frequently used, this is due to the various volumes of solutions in the different stages of experiments (the various volumes arise from different s/l-ratios). The use of mass and efficiency are more applicable/convenient for the sake of comparison, [g/L] is therefore only used in cases where the volumes are equal, and values can be compared. Raw data from MP-AES analysis (mg/L) can be found in Appendix A. Regarding the discussion of leaching experiments, the terms "leaching" and "dissolution" are considered equivalent and will be used extensively. URLs to all Excel worksheets with raw data are included in Appendix D.

3.1. Composition of Spent Cathode Material

The spent electrode material (pre-treated EOL LIBs) was used in dissolution experiments with inorganic and organic acid (Section 2.4 and 2.5). To calculate the efficiencies of the experiments, an initial determination of electrode composition was performed.

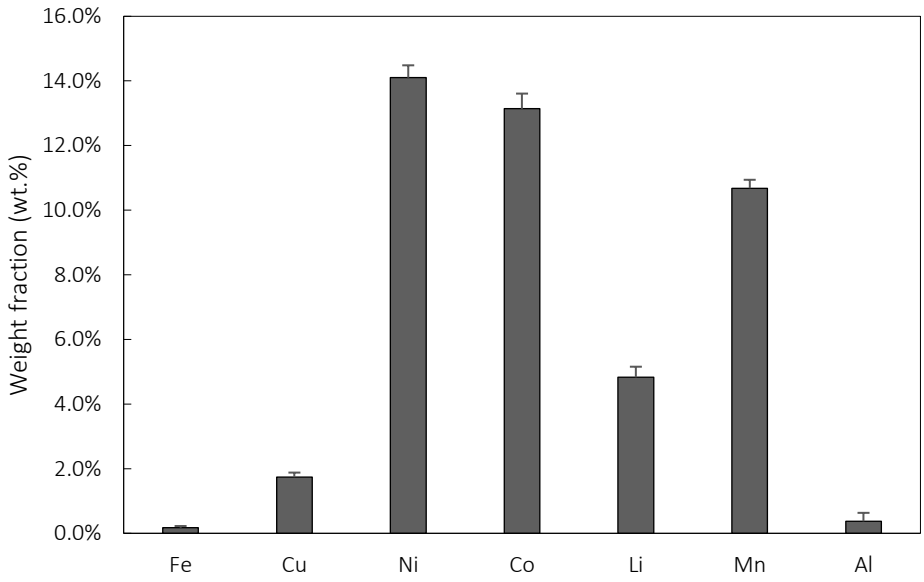

Figure 3.1. Weight percentage of metals in black mass.

The bar chart above provides the metal composition of the initial black mass form spent, pre-treated LIBs, and are constructed from the digestion of solid sample followed by MP-AES analysis. The procedure for digestion experiments is presented in section 2.3. The wt.% are

average values calculated from the mass of metals in three samples obtained by digesting different solid amounts, a calculation example can be found in Appendix B.

As seen from the diagram (Figure 3.1) Ni, Mn, and Co are the dominating metals present in the electrode waste, any one of them make up a fraction >11 wt.%. The presence of these three metals and the similar wt.% indicates that this might be a cathode of the NMC type (Section 1.1)[4]. Apart from Ni, Mn, and Co, Li is also of abundance. Lithium derives from the mixed metal oxide of the spent battery and the conductive salt of the electrolyte. The traces of copper and aluminium arise from current collectors (e.g., Al_2O_3 coating) in commercial NMC cathodes [18], while iron might be an impurity from steel casing [4, 27]. The short error bars (from low SD values) indicate that the samples were fairly homogeneous and that the digestion with subsequent with following filtration process are efficient. The remaining wt.% are mainly carbon, along with fluoride, phosphor and sulphur from cell casings, electrolytes, and binders [4].

By comparing the wt.% obtained (Figure 3.1) to those of ICP-OES analysis (Table 2.2 in Section 2.1) done by Aachen University, only minor differences can be seen. The small deviations are below 1% and may arise from sample preparations or inhomogeneity in the sample due to grain size.

3.1.1. Predicting Elemental Ratio of (Cathode) Mixed Metal Oxide

From the content of metals in the black mass, one can predict the metal ratio of the cathode. The cathode mixed metal oxide is commonly used to name the batteries based on the weight fraction the respective metals make up, like NMC-532 ($Ni_{0.5}Mn_{0.3}Co_{0.2}$) [4]. As a continuation from the previous section (Section 3.1), the metal composition was used to determine the elemental ratio between Ni, Mn, and Co, and thus predict the type of cathode. As mentioned above, one can believe that the cathode is of the NMC type.

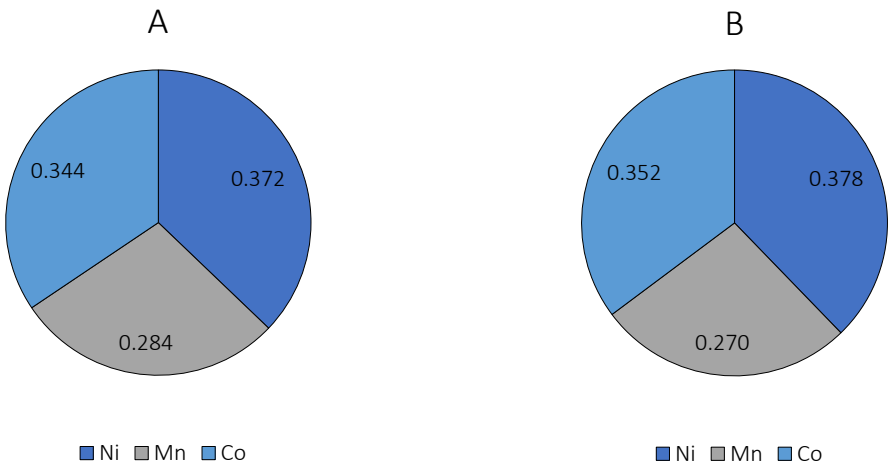

Figure 3.2. Weight fraction of Ni, Mn and Co in black mass from (a) MP-AES and (b) XRF analysis.

Pie charts (a) and (b) represent the weight fraction on Ni, Mn, and Co in the black mass provided from MP-AES and XRF analysis, respectively (Figure 3.2). A filtered suspension of black mass in aqua regia is the basis for the MP-AES analysis, whereas a dry fraction of the same powder is used directly for metal detection via XRF. All values are weight fractions (wt.%), a calculation example for the digested sample can be found in Appendix B. XRF provides normalized mass fractions of all detected components, and the values of Ni, Mn, and Co are normalized from these (URL to the Excel sheet can be found in Appendix D).

From MP-AES analysis are calculated a mass-based elemental ratio of $Ni_{0.34}Mn_{0.28}Co_{0.37}$. The corresponding XRF examination gives a $Ni_{0.35}Mn_{0.27}Co_{0.38}$ ratio, the results are coherent. The predicted ratio is consistent with previous research [18, 33, 36]. Minor differences in wt.% may arise from dissimilar sample preparation or the inhomogeneity of each sample (as the grain size is 0-0.25 mm). For the digested sample, minor loss of metals during the filtration step of the aqua-regia suspension is likely. Regarding the solid sample for XRF, only a small amount of powder is used, and it is reasonable to assume that the grain size could be affecting the measurement. A small fraction of the bigger sample might not be representable for the whole, due to increased chances of inhomogeneity. Moreover, the sensitivity of Agilent MP-AES is reported down to sub-ppb levels, whereas the Rigaku XRF announce “low concentration levels” [32, 37].

3.1.2. Phase Identification of Spent Electrode Material

An XRD analysis of the initial black mass was conducted, resulting in the pattern presented below.

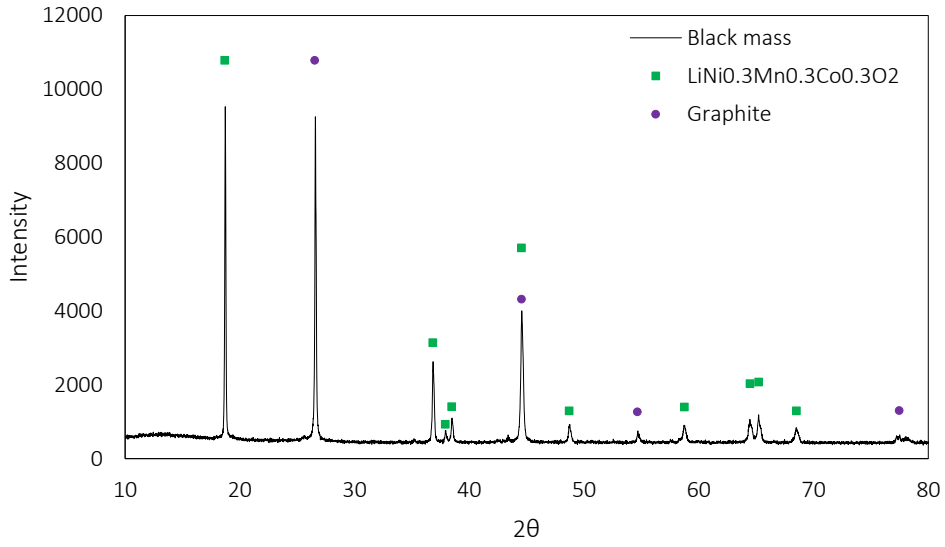

Figure 3.3. XRD pattern from analysis of initial black mass.

The figure above is composed of a solid sample XRD analysis of the black mass and the ICDD database [38]. Measurement conditions for this high crystallinity sample can be found in section 2.2. The presented XRD pattern (Figure 3.3) indicates that the initial black mass is composed of the mixed metal oxide $LiNi_{0.33}Mn_{0.33}Co_{0.33}O_2$ (PDF 00-062-0431) [38]. Furthermore, the phase identification confirms the presence of carbon (PDF 00-056-0159) [38] from the graphite anode.

The result coheres with the previously calculated wt.% from MP-AES and XRF analysis (Figure 3.2 in Section 3.1.1), and confirms the assumption of a 1:1:1 ratio between the metals Ni, Mn, and Co. Furthermore, the detected phases are consistent with previous research and theory, at it can hereby be confirmed that the black mass is a mixture of the anode and $N_1M_1C_1$ cathode (Section 2.1) [4, 18]. Furthermore, treating the electrode as a whole will contribute to meeting the goal of a higher level of automation.

Both MP-AES analysis after digestion and XRF of the solid phase give weight fractions in a ratio equivalent to $Ni_1Mn_1Co_1$, this corresponds to the phase characterization from XRD given in the present section (Section 3.1.2).

3.1.3. Examining Particle Morphology of Spent Electrode Material

To investigate the particle morphology of black mass, SEM was employed.

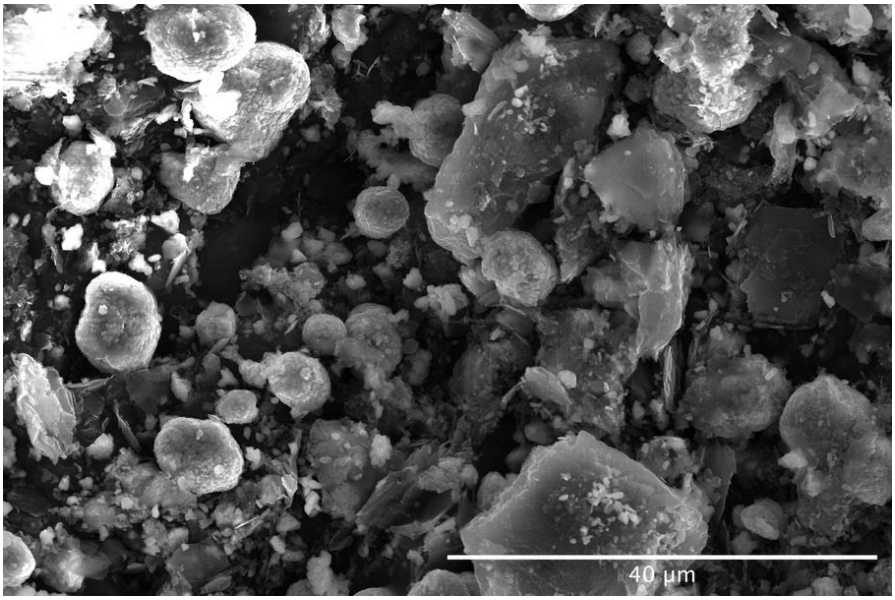

Figure 3.4. SEM image of spent electrode material.

From this top-view SEM image (Figure 3.4) it can be seen large aggregates of electrode material. A small fraction of the solid sample was added to a conductive tape and examined via SEM (in standard lens mode, beam current of 0.4nA and accelerating voltage of 20kV). The spent NMC cathode can be observed as spherical particles with sizes of ≈5-7 µm, while the grey, layered structure is traces of carbon from the anode [18, 39].

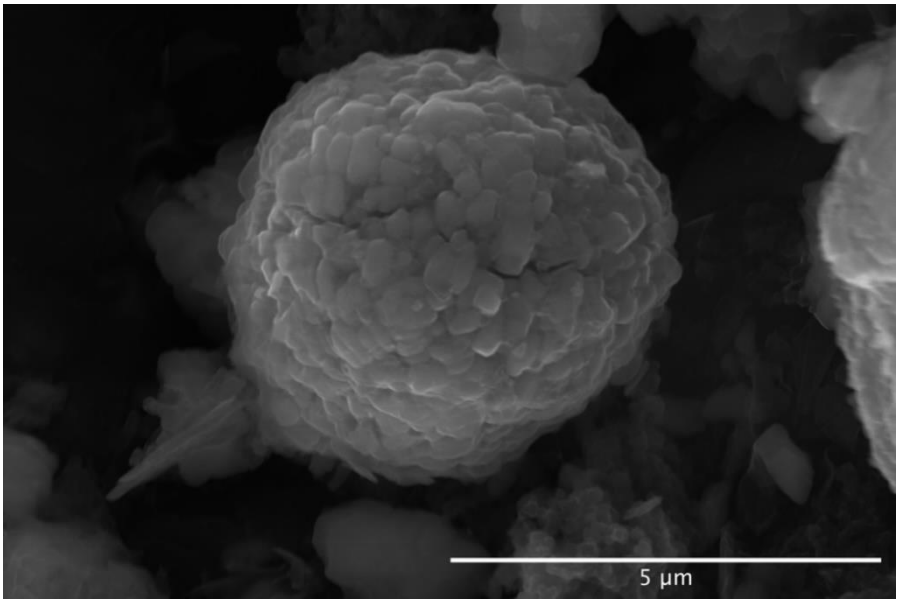

Figure 3.5. Magnified view of spent electrode material.

Above can be seen a high magnification image of a spherical NMC particle (Figure 3.5). The same conditions are used in terms of beam current and accelerating voltage as the top-view image (Figure 3.4). The size of this individual particle is ≈ 5 µm, but from the image above one can see how the sizes vary throughout the sample. The spherical grain orientation may arise from the hexagonal structure of an NMC particle. The hexagonal unit cell allows for 12 possible symmetries (various orientations), this may explain the variation in particle morphology seen in the low magnitude image (Figure 3.4) [40]. Although there is not done EDS mapping to confirm that the particle is made up of the suggested metals (Ni, Mn, and Co), the morphology and comparison to similar research firmly indicate that the particle is of the NMC type [18, 40, 41].

3.2. Sulfuric Acid Leaching

An initial sulfuric acid leaching was performed to discover how the s/l-ratio and the presence of a reducing agent affected the dissolution of metals. The outcome was further used to select the conditions for the subsequent dissolution step of solid residues after oxalic acid leaching. Results from inorganic acid leaching are presented below, the raw data in terms of concentration of metals (mg/L) in all leachates can be found in Appendix A

3.2.1. The Effect of Reducing Agent on Metal Dissolution

The presence of hydrogen peroxide in sulfuric acid leaching was investigated, results are presented below.

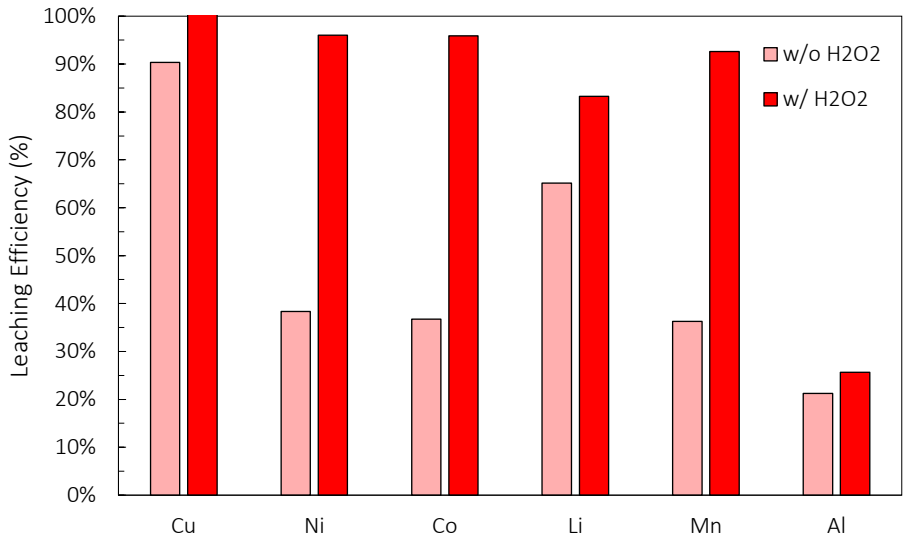

Figure 3.6. Leaching efficiency of metals with and without reducing agent. Conditions: 50g/L 80˚C.

Provided bar chart (Figure 3.6) illustrate the effect of reducing agent on leaching efficiency for Cu, Ni, Co, Li, Mn, and Al. The reductant used is hydrogen peroxide. The metals are detected and quantified by the use of MP-AES, and efficiencies are calculated from the mass of metal in the black mass and the resulting leachate solutions. Leaching conditions and methods are found in section 2.4.

An uneven distribution of leaching efficiencies is depicted from the various heigh of the light red bar, ranging from 21-90%. For the bright red bars, the trend evens out. For Ni, Co, and Mn can be seen a significant increase with the use of a reductant. For all three metals, a percentage increase of >150% is demonstrated. The efficiency with respect to lithium increases by 30% from 56- 83%, whereas only a minor rise is noticed for Cu and Al. An increase in weight loss ($m_{\text{black mass}} - m_{\text{filter residue}}$) was also seen with the use of hydrogen peroxide, this is consistent with the higher dissolution efficiency (as the metals convert from solid- liquid state).

The chemical reaction equation below demonstrates how the NCM reacts with sulfuric acid in the presence of H_2O_2 [20]:

$$6LiNi_{0.33}Mn_{0.33}Co_{0.33}O_2 + 9H_2SO + H_2O_2 \rightleftharpoons$$

$$2MnSO_4 + 2NiSO_4 + 2CoSO_4 + 2LiSO_4 + 10H_2O + 2O_2 \qquad (1)$$

Hydrogen peroxide aids the leaching in terms of transforming the metals into their divalent state, for instance, Co(III) to Co(II), which enhances the solubility in acidic solutions [2, 15, 19]. Compared to the literature, the overall efficiencies with the use of H_2O_2 are respectable. From previous research, it is demonstrated efficiencies > 98.5% for all cathode metals [20, 42]. The temperature of 80˚C could have induced degeneration of H_2O_2, due to the instability of the reducing agent at high temperatures, this increases the efficiency [14]. The lower efficiencies obtained for Mn and Co, without the attendance of reducing agent might be due to their presence in higher valence state (e.g., Mn^{4+} and Co^{3+}) [24].

3.2.2. The Effect of s/l- ratio on Lithium Dissolution in Inorganic Acid

The effect of s/l-ratio and the presence of a reducing agent is shown in figure 3.7. The leaching efficiency with respect to lithium decreased as the s/l-ratio increased. Lower liquid ratios of 30 g/L and 50 g/L provides the same mass-wise dissolution. The highest efficiency of 83 % can be noticed from the 50 g/L experiment with H_2O_2. At 50 g/L, a percentage increase of 30% can be calculated upon the use of H_2O_2. However, the flat trend indicates that the s/l-ratio is not of great significance.

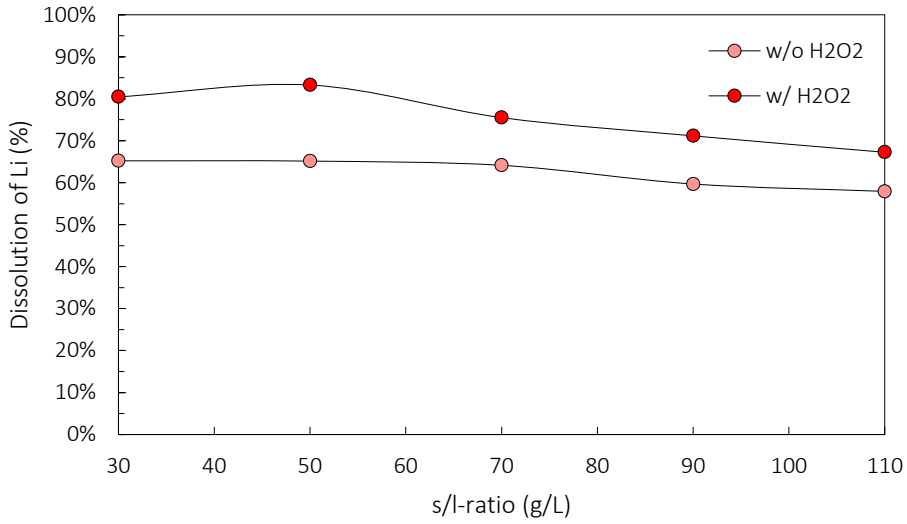

Figure 3.7. Effect of s/l-ratio and reducing agent on Li dissolution.

The use of H_2O_2 demonstrated increased efficiency for all metals, whereas the increase in s/l-ratio induced a slight decline in dissolution percentage. A lower s/l-ratio is equivalent to a greater contact area between a solid material and the liquid, by means of making the soluble portions more accessible to the acid, which in turn will increase the dissolution. Results coincide with the literature [20, 43]. Although a low s/l-ratio yields the highest efficiency, it would generate greater costs due to the higher volumes of solvent. There is a trade-off between costs and recovery rates. From an industrial point of view, a moderate s/l-ratio is desired as it will provide both high production capacity and sufficient recoveries at a reasonable cost.

3.3. Oxalic Acid Leaching

Organic acid dissolution experiments were designed by the use of JMP DOE (Design of Experiments). The Definitive Screening Design was applied to discover which factors had a substantial effect on the response (lithium concentration) and how the factors (temperature and s/l-ratio) affected one another. By adding a range of s/l – ratios and temperatures, a design consisting of 13 randomised experiments was computed. The different s/l -ratio and temperature in each experiment were used to determine how they affected the lithium content in the resulting solutions. Duplicates were also included to consider replicability. The JMP "Fit Definitive Screening" feature computed a prediction profiler which depicted the main effect of temperature (Figure 3.8), s/l-ratio was found to be insignificant.

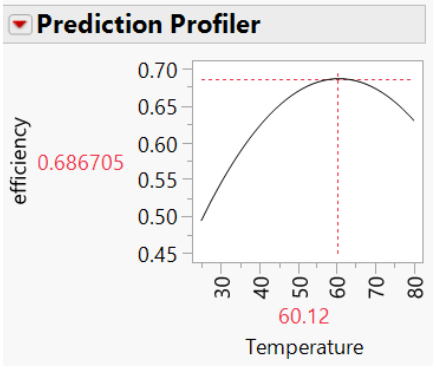

Figure 3.8. Result from "Fit Definitive Screening" by using JMP.

Results from the experiments are presented in the diagrams below. The effect of various operating conditions, in particular solid-liquid ratio and temperature is discussed in the following sub-sections. The concentration of metals in leachates can be found in Appendix A.

3.3.1. The Effect of s/l-ratio and Temperature on Lithium Dissolution

A summary of screening experiments (Table 2.4) is presented in the figure below (Figure 3.9), and it can be seen how the s/l-ratio (a) and temperature (b) affect the leaching efficiency with respect to lithium. The leaching procedure can be found in section 2.5, whereas calculation examples are provided in Appendix B. The highest efficiencies are resulting from experiments performed at 53˚C, with values of 63% and 62% for s/l-ratios of 30 g/L and 70 g/L, respectively. The lowest efficiency can be observed for the attempt of 7.5 g powder in 0.068 L (i.e., 110 g/L) of acid at 25˚C, leading to a value of 36%.

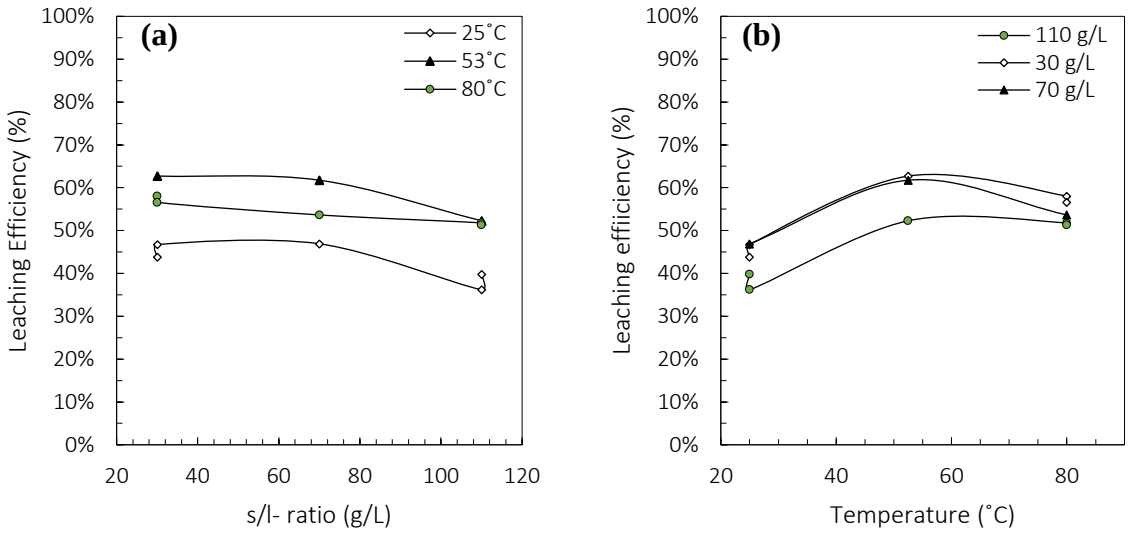

Figure 3.9. Leaching efficiency of Li for different s/l-ratios (a) and temperatures (b).

The flat trend indicates that the s/l-ratio is not of great significance. However, a maximum can be seen for an s/l-ratio of 30g/L and 70g/L at 53˚C. The increase in temperature does not pose an increase in the leaching performance, considering the highest efficiency is seen for the 53˚C experiments. The trend of temperature is similar to the one composed from JMP prediction profiler (Figure 3.8). Taking into account the effect of s/l-ratio at 80˚C, the marginal impact can be seen from the flat trend. With regards to s/l-ratio, the marginal impact of s/l -ratio coincide with the outcome of the previous section 3.2.2, and the result from JMP definitive screening.

Although s/l-ratio of 30g/L and 70g/L provided the same efficiency, a higher s/l-ratio is favoured in terms of enhanced production capacity and lower operational costs, seen from an industrial perspective. For this reason, conditions of 70 g/L and 53˚C were selected for further experiments.

3.3.2. Investigating Replicability of Leaching Experiments

From the previous section (Section 3.3.1) it was discovered that a s/l-ratio of 70g/L and temperature of 53˚C provided the highest dissolution efficiency with respect to lithium. For that reason, these conditions were chosen for further experiments. In order to aid the subsequent precipitation step by means of a high lithium concentration (thus, enhanced conditions for supersaturation to occur), no dilution was done [26]. The replicability of experiments is investigated to ensure trustworthy replicates.

Table 3.1. Average metal concentration in eight replicates of oxalic acid leachates. Conditions: 70g/L, 53˚C.

	METAL CONCENTRATION IN LEACHATE (mg/L)						
	Fe	Cu	Ni	Co	Li	Mn	Al
Avg.	63	25	9	28	2524	90	124
STD	11	3	1	3	93	3	4
RSD	17%	13%	15%	11%	4%	4%	4%

Average metal concentrations in eight replicates of oxalic acid leachates are presented in the table above (Table 3.1). The leaching procedure is explained in section 2.5, and the concentrations (mg/L) are detected by the use of MP-AES. Standard deviation is calculated from the eight repeats, and the relative standard deviation indicates its significance compared to the mean values. In other words, a measure of how closely clustered the data set is to the main value [44].

For Fe, Cu, Ni, and Co the values are of significance (>5%), whereas for the remaining metals (Li, Mn, and Al) they are 4%. In the bigger picture, only Li is of interest in this stage of the process. All other metals are anyhow present in low concentrations and considered as impurities. Furthermore, they will primarily be removed in the subsequent precipitation step. For that reason, replicability can be considered sufficient.

3.3.3. Examining the Impact of Colour Change after Filtration

A colour change in solutions was observed for all leachates, especially the experiments performed at 25˚C (Figure 3.10). An MP-AES analysis of the respective solutions was done to determine whether the composition and/or concentration of metals were affected by the variation in colour, the result is presented in table 3.2.

Figure 3.10. Colour change in leachate solution (a) 0 hr, (b) 0.3 hr and (c) 1 hr after filtration. Conditions: 110 g/L, 25˚C, 2.5 hours reaction time.

Table 3.2. Metal concentration in acid leachate after different rest times. Leaching conditions: 25˚C, 110 g/L.

	METAL CONCENTRATION IN LEACHATE (mg/L)						
Time (h)	Fe	Cu	Ni	Co	Li	Mn	Al
0	85	20	81	36	2664	318	189
0.3	60	17	79	33	2581	309	178
1	56	15	74	31	2398	289	168
Avg. ± SD	67 ±13	17 ±2	78 ±3	33 ±2	2548 ±111	305 ±12	178 ±9
RSD	20%	14%	4%	5%	4%	4%	5%

From the pictures (Figure 3.10) it can be seen how the colour changes from bright red to green after 1 hour of rest. This transformation was only seen in solutions of experiments conducted at 25˚C. Solutions from leaching experiments done at 53˚C and 80˚C only had a slight colour change from bright green to a rather light green/yellow colour.

The colour change might be due to the oxidation of metals. Solid nickel- and copper oxalate salts are both blue/green in colour, whereas cobalt oxalate is red [45, 46]. Furthermore, the oxalate anion in an aqueous solution is demonstrated to provide a reddish colour. From the poorer efficiencies observed at 25˚C (Figure 3.9 in Section 3.3.1), unreacted oxalic acid might be the reason for the red colouration [47]. The colour change (green-yellow) seen in 53˚C and 80˚C experiments, could be a result of the reduction of iron from Fe^{3+} to Fe^{2+}. Ferric oxalate is green, whereas iron oxalate is yellow, this could potentially cause the shift in colour from bright green to yellow [47, 48]. Oxalic acid is known to be a mild reducing agent [15, 17], and the reaction might have proceeded after filtration. The assumption that iron causes the solution colour, is consistent with the high co-dissolution of Fe seen in the oxalic acid leachates (Figure 3.15).

The table presents the concentration of metals in the solution after 0-, 20-, and 60-minutes rest, respectively (after dissolution in room temperature, s/l-ratio of 110g/L) (Table 3.2). For iron and copper, it can be noticed an RSD value of 20% and 14%, respectively. The remaining metals has an RSD of 4-5%, indicating that they are closely aggregated to the mean (average) value.

The one high value for Fe (0h), can be due to deviation in the 1 mL of sample used for measurement from the remaining solution and might arise from poor mixing (i.e., inhomogeneity) prior to sampling. For Fe and Cu, the relative standard deviation (RSD > 5%) shows that the rest time is of significance (given $\alpha = 0.05$) [44]. Traces of copper are residues

from the current collectors, while iron impurities may arise from steel cell casing. The presence of both metals is below the impurity limit of 100 ppm [4, 27].

RSD values for lithium and remaining metals (4-5%) are not significant, and for this reason, one can assume that the colour change after filtration did not affect the concentration. However, solutions resulting from 25˚C experiments did not have a high efficiency towards lithium and are not used in further experiments. Nonetheless, to ensure trustworthy measurements, leachate solutions from the following experiments are left to rest more than 1 hr after filtration prior to analysis.

3.3.4. Characterization of Solid Residue after Selective Lithium Dissolution

Filter residues from the oxalic acid leaching were analysed with XRD, the resulting pattern is presented below.

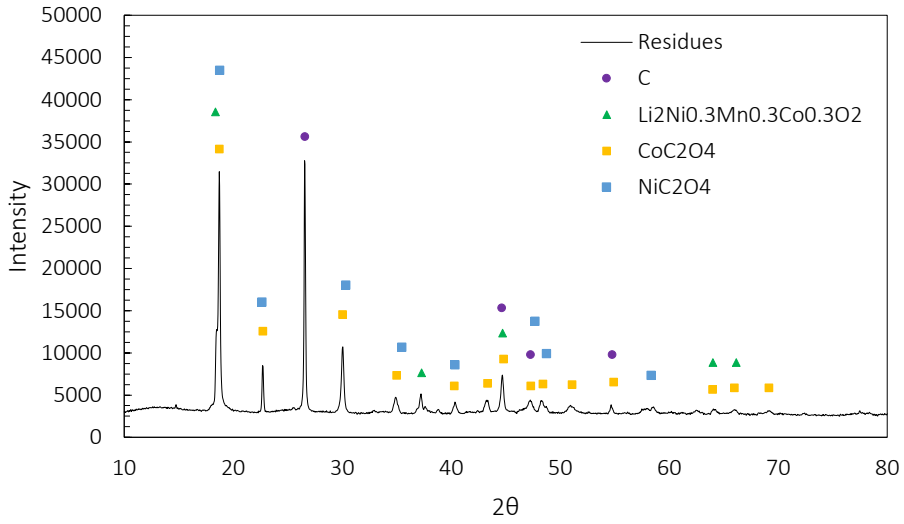

Figure 3.11. XRD pattern of solid residue after 1.st (oxalic acid) leaching/ selective lithium dissolution. Conditions: 70g/L and 80˚C.

Figure 3.11 shows the XRD pattern of leaching residues after oxalic acid leaching (O-80-70) and are composed of solid sample XRD analysis. The range of 2θ is selected to 10-80˚, additional measurement conditions can be found in section 2.2. The 2θ parameter is determined from the database [38], by means of where peaks of carbon, mixed metal oxides and cobalt oxalate could be expected, besides investigating XRD patterns from similar research [16].

The presence of unreacted carbon from the anode are confirmed by the peaks at 27, 45 and 55 (and purple dots) (PDF 00-056-0159) [38] [42]. The peaks with an intensity of ≈10,000 at an angle of 22 and 30, corresponds to α-oxalate, this indicates that metal oxalate precipitates were formed in the leaching experiment [16, 18, 43]. Intensity peaks below yellow squares display

cobalt oxalate (PDF 04-016-6937), while the blue ones correspond to nickel oxalate (PDF 00-025-0581) [38]. Although the database applied do not have any pattern for manganese oxalate, from patterns in similar research papers one can prove/assume the presence of it. It is believed that the oxalic acid will react with the black mass to form metal oxalates in a solid and liquid state, by the following reaction equilibrium (Section 1.5) [18]:

$$4H_2C_2O_4 + 2LiNi_{0.33}Mn_{0.33}Co_{0.33}O_2 \rightleftharpoons$$

$$Li_2C_2O_4 + 2(Ni_{0.33}Mn_{0.33}Co_{0.33})C_2O_4 + 4H_2O + 2CO_2 \qquad (2)$$

Table 3.3. Concentration of metals in leachate O-80-70.

	Concentration of metals (mg/L)						
No.	**Fe**	**Cu**	**Ni**	**Co**	**Li**	**Mn**	**Al**
O-80-70	55.4	61.7	2.0	11.6	2113.3	204.5	127.2

Apart from minor co-dissolution of Mn and Al, MP-AES analysis of the associated leachate (Table 3.3) confirms that Li was selectively dissolved, meaning that the solid residue should contain remaining metals. Additionally, the increase in weight of the filter residue (the filter cake is of greater mass than the initial weight of black mass added to the reactor) indicates that some precipitates are formed during the leaching process. Normally, the mass will decrease due to the dissolution of metal from solid to a liquid state, but this case demonstrates an opposite trend. From the increase in mass, the fact that metal oxalates are insoluble in acidic media (i.e., will precipitate [17, 32], and the detection of oxalate phases by XRD it is reasonable to assume that the filter residue is a mixture of unreacted black mass (metal oxides) and metal oxalates.

3.3.5. Increased Lithium Recovery by Subsequent Inorganic Leaching

Below is presented an overview of metal dissolution through the two stages of leaching (oxalic acid and subsequent sulfuric acid leaching).

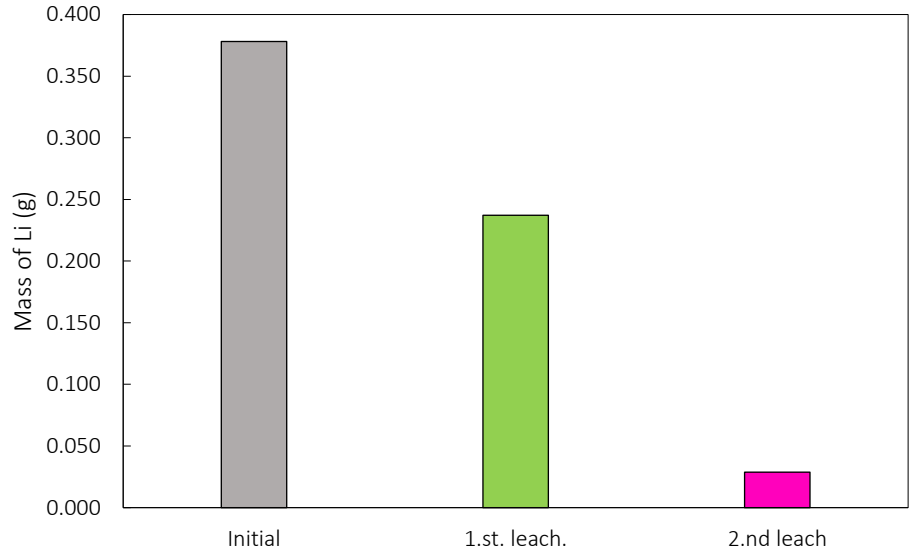

Figure 3.12. Mass of lithium in initial black mass, 1.st leachate and 2.nd. leachate. Conditions for leaching: 30g/L, 53˚C and 110g/L, 80˚C, respectively.

This diagram (Figure 3.12) depicts the mass of metal in the initial black mass, the first leachate (Section 2.5) and the second leachate (Section 2.5.1) by grey, green and purple bars. The mass of metals is calculated from leachate solutions quantified by MP-AES. The green bar demonstrates that the majority of Li (0.237g out of 0.378g, i.e., 63%) is leached out during the oxalic acid leaching. By adding up the bars to get the total Li recovery from the individual solutions, one gets an overall efficiency of 70 %. This indicates a successful dissolution of Li by the use of oxalic acid. The result coincides with previous research performed by Li et al. (C= 1, s/l= 30g/L gave an efficiency of ≈ 80%), although that experiment was conducted at 80˚C for 12 hours [16]. The result respect to a selective Li leaching is presented below.

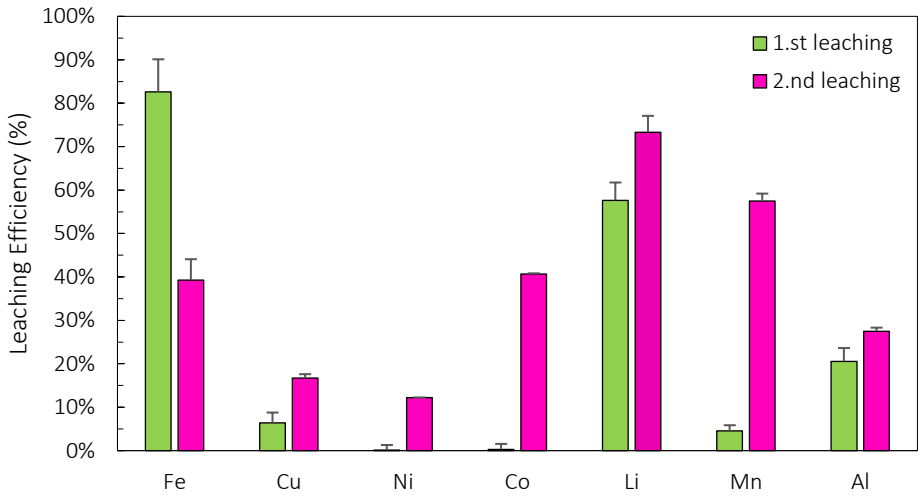

Figure 3.13. Leaching efficiency of all metals for oxalic acid leaching and subsequent sulfuric acid leaching. Conditions: 30-70 g/L and 53-80˚C (1.st). 110 g/L 80˚C (2.nd.).

The diagram (Figure 3.13) are constructed from leaching experiments and following MP-AES analysis of leachate solutions. Leaching procedures are explained in section 2.5 and 2.5.1. Efficiencies are calculated based on the mass of metals in the solid sample (black mass or filter residue) used in the experiment, and in the resulting leachate solution (calculation examples can be found in Appendix B. The composition of initial solid samples can be found in section 3.1 and 3.3.4.

Apart from the high, green bar of Fe, the figure depicts how lithium is selectively leached out in the dissolution experiment. Some Al and Mn are present in low amounts. Uneven distribution in leaching efficiency for the different metals are seen from the purple bars. In particular, the Ni efficiency is greatly reduced (70%) compared to the initial inorganic acid leaching (Figure 3.6). Cu efficiency remains the same, whereas Mn increases by 63%. An s/l-ratio of 110 g/L was chosen with regards to an industrial approach, this would yield a high production capacity and reduced costs.

Ni, Mn and Co oxalates are reported to be insoluble, while Li is dissolved in the solution [18]. Precipitation and dissolution reactions can take place by the reaction equilibrium presented in the previous section 3.3.4. Low presence of these metals (Ni, Mn, and Co) in the leach liquor after the first leaching is thus consistent with theory. Moreover, iron and aluminium will react with oxalic acid and forms soluble complexes according to the equations below [48].

$$Fe^{3+} + 3{C_2O_4}^{2-} \rightleftharpoons Fe(C_2O_4)_3^{3-} \quad (7)$$

$$Al^{3+} + 3{C_2O_4}^{2-} \rightleftharpoons Al(C_2O_4)_3^{3-} \quad (8)$$

Whereas Fe^{3+} is found to be very stable in oxalic acid solution, the reduced Fe^{2+} has a very slight solubility ($K_{sp} = 3.2 \cdot 10^{-7}$). For that reason, reducing Fe^{3+} into the insoluble Fe^{2+} will enhance the precipitation as from the following reaction equation:

$$Fe^{2+} + Fe(C_2O_4)_2^{2-} + 4H_2O \rightleftharpoons 2FeC_2O_4 \cdot 2H_2O \downarrow \quad (9)$$

Excess oxalic acid might increase the precipitation by means of enhancing its reduction potential towards the metals [48, 49]. Furthermore, the solubility product constant of manganese oxalate ($K_{sp} = 1.7 \cdot 10^{-7}$) is very similar to the one of ferric oxalate, this might be the reason for its minor co-dissolution. In regard to the subsequent leaching, it is demonstrated that FeC_2O_4 $2H_2O$ can be dissolved in solution as it converts into $FeSO_4$ H_2O through subsequent inorganic leaching [48]. This is coherent with the depicted result (Figure 3.13).

The coordination of Ni^{2+} to the oxalate anion results in a five-membered ring structure, which is of strong character [18]. However, it has been demonstrated that Ni^{2+} in the presence of H_2SO_4, H_2O_2, and oxalate can form soluble complexes as it is oxidised by the H_2O_2 to a higher valence state [50], this contradicts the poor efficiency observed.

Although the initial sulfuric acid leaching was performed to discover how s/l-ratio and the presence of reducing agent affected the dissolution of metal oxides, the dissolution of metal oxalates might differ from this. The same efficiencies cannot be expected, as there are different reactions occurring and the oxalic acid are known as an excellent ligand to bind metal ions, which in turn could complicate the dissolution reaction. A comparison of inorganic acid leaching of initial black mass and filter residue is examined in the following section.

3.3.6. Characterization of Solid Residue after Dissolution of Remaining Cathode Material

Filter residues of the subsequent inorganic leaching of solid residue from organic acid leaching were analysed with XRD, the resulting pattern is presented below.

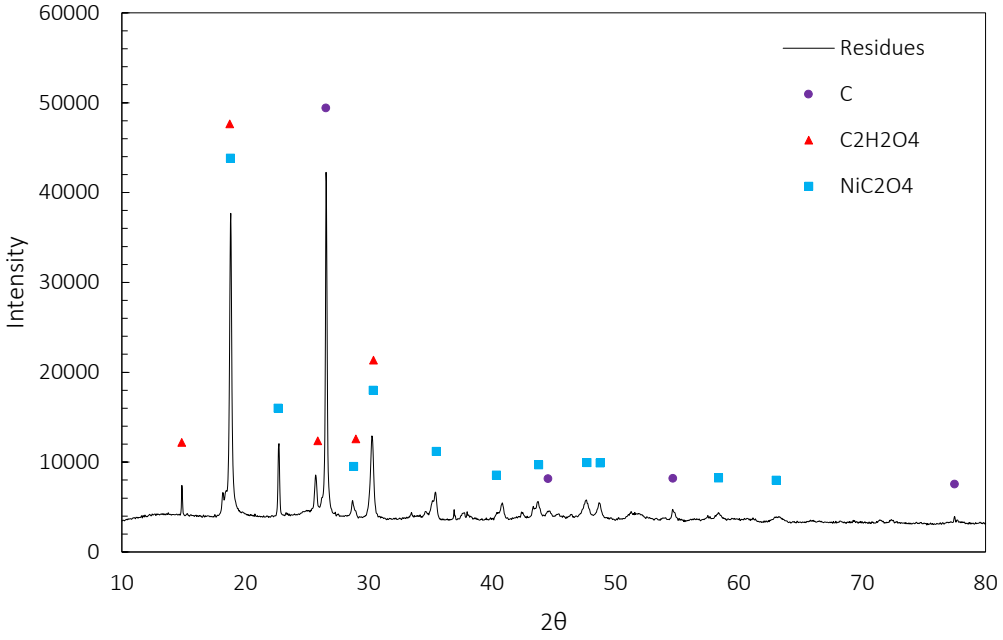

Figure 3.14. XRD pattern of solid residue after subsequent inorganic leaching. Conditions: 110g/L and 80˚C.

From figure 3.14 can be seen an XRD pattern of solid filter residues after inorganic acid leaching of unreacted black mass and metal oxalates (i.e., residues from O-80-70) (Section 3.3.4). The leaching procedure is explained in section 2.5.1. To ensure a satisfactory pattern from the sample of unknown nature, it was assumed to be of low crystallinity. The step size and step time are adjusted accordingly (measurement conditions can be found in section 2.2). The range of the 2θ parameter was predicted from the database of compounds to be expected [38].

The existence of carbon from the unreacted anode material is indicated as purple dots above the intensity peaks at ≈ 27, 45 and 55 (PDF 00-056-0159) [38]. The peaks at 2θ ≈ 15, 19, 26 and 30 correspond to the presence of oxalic acid (PDF 00-014-0832) [38]. Oxalate in the form of nickel oxalate is also present in the sample, indicated by blue squares above the intensity peaks (PDF 00-025-0581) [38]. The result indicates that nickel oxalates were not completely dissolved during the leaching experiment. Calculated leaching efficiency of Ni from MP-AES analysis of the associated leachate (Section 3.3.5), confirm the poor dissolution rate of nickel. This is consistent with the traces of Ni seen in the solid residue. The presence of oxalic acid may arise from unreacted oxalic acid or regeneration of the acid as the metal oxalates convert into metal sulphates metal oxalate react with sulfuric acid to form metal sulphate, and thus a

release of H^{2+} which react with the oxalate base and regenerates the oxalic acid), as described by the reaction equation below [20]:

$$MC_2O_4 + H_2SO_4 \leftrightarrow H_2C_2O_4 + MSO_4 \quad (10)$$

3.3.7. The Effect of Metal Oxalates on Inorganic Leaching Efficiency

This section provides a comparison of the initial and subsequent inorganic acid leaching.

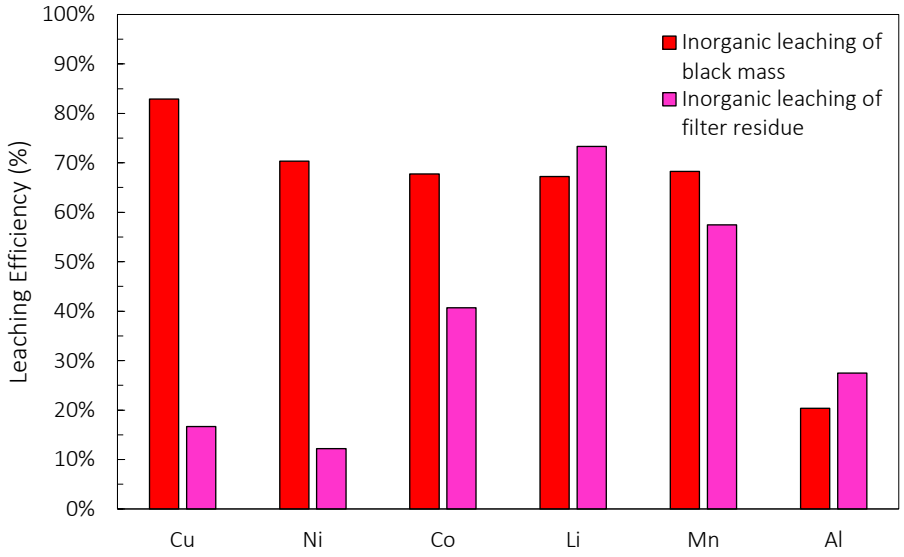

Figure 3.15. Leaching efficiency (%) of metals from black mass and filter residues with the use of sulfuric acid. Conditions 110g/L, 80˚C, 2M H_2SO_4.

The bar chart (Figure 3.15) shows inorganic acid leaching of black mass and filter residue from the oxalic acid leaching, presented as red and pink bars, respectively. Leaching efficiencies are calculated from the mass of metals in solutions after dissolution experiments using MP-AES (Appendix B). From the red bars, it can be seen an even leaching efficiency of 67-83% with respect to all metals apart from Al, with a lower value of 27%. From the use of inorganic acid in the subsequent leaching step (of solid residues from section 3.3.1), the efficiency is considerably lower for metals Cu, Ni, and Co. However, for Li and Al it increases by 9% and 35%, respectively. Pink bar of Mn efficiency depicts a slighter decrease. The poor dissolution of Ni in the subsequent leaching is confirmed by the presence of NiC_2O_4 in the filter residues (Figure 3.14 in Section 3.3.6).

3.4. Comparing Leaching Media

To illustrate the selective dissolution of lithium with the use of oxalic acid, it was compared to an experiment using sulfuric acid (Section 2.4) under the same experimental conditions. The following diagrams depict the effect of leaching media on selective lithium dissolution.

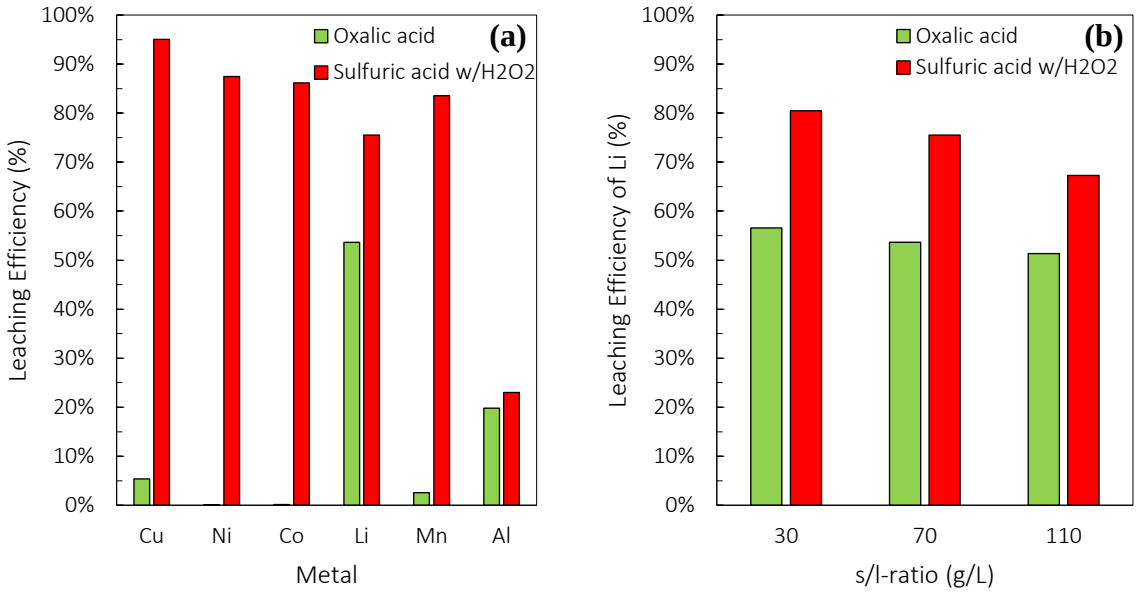

Figure 3.16. Leaching efficiency of (a) all metals and (b) lithium using oxalic acid and sulfuric acid. Conditions 70g/L and 80˚C, 1M $H_2C_2O_4$ and 2M H_2SO_4+ 3.75% H_2O_2.

A comparison of metal dissolution through sulfuric acid leaching and oxalic acid leaching of black mass is provided in the bar chart above (Figure 3.16a). How the s/l-ratio affects the Li dissolution with respect to leaching media is shown in figure 3.16. Mass-based efficiencies are calculated from the concentration of metals in leachate solutions analysed by MP-AES.

The red bars depict efficiencies from metal dissolution in inorganic media (Figure 3.16a). Apart from the lower efficiency with respect to Al (23%), it can be seen how all the metals are leached out in similar dissolution rates (76-95%). Green bars present the effectiveness of leaching using oxalic acid. Although some Al is co-dissolved, a selective dissolution is demonstrated by the one taller bar (of Li) from the remaining ones (<5%). A suggested explanation of the Al-dissolution is presented in section 3.3.5. The minor dissolution of Mn could be due to the higher solubility of manganese oxalate (K_{sp} = $1.7 \cdot 10^{-7}$), compared to NiC_2O_4 (K_{sp} = $7.8 \cdot 10^{-10}$) and CoC_2O_4 (K_{sp} = $2.7 \cdot 10^{-9}$) [18, 29]. The reaction equation of the dissolution of NMC in oxalic acid is presented in section 3.3.4.

Figure 3.16 (b) is of the same nature as figure (a), though with an emphasis on lithium and the effect of varying s/l-ratio. As observed from the left-hand figure, the use of oxalic acid provides

an overall lower leaching efficiency. This chart indicates that the noticed decrease in dissolution rate by the use of oxalic acid, are valid for all the s/l-ratios examined. By increasing the solid-liquid ratio from 30 g/L to 110 g/L the leaching performance decreases by 11 %. The corresponding decrease with the use of sulfuric acid is calculated to 15%. The decreasing dissolution might be due to decreased contact area or shortage in excess acid [20]. An individual discussion of oxalic acid and sulfuric acid dissolution can be found in section 3.2 and 3.3.

3.5. Removal of Metal Impurities by Chemical Precipitation

Only oxalic acid leachates are used for precipitation experiments, and all metals apart from lithium are considered impurities. NaOH and NH_4OH are utilized as precipitation agents in the attempt to remove impurity metals (all metals except for Li) as hydroxides. After crystallization of metal hydroxides, the solutions are filtered and added Na_2CO_3 to selectively precipitate lithium as lithium carbonate (Figure 3.17). Precipitation of metal hydroxides is performed at a temperature of 60˚C. Due to the lower solubility of Li_2CO_3 at high temperatures, the second precipitation is performed at 90˚C [14, 16]. Below is presented the results from experiments of removal of impurities and selective Li precipitation.

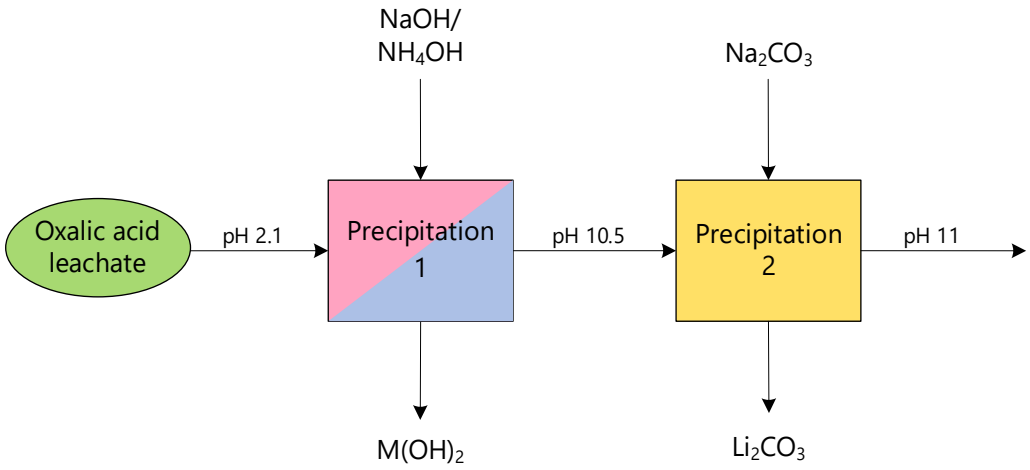

Figure 3.17. Flow sheet for two precipitation steps using $NaOH/NH_4OH$ and Na_2CO_3.

3.5.1. The Effect of Precipitant on Impurity Removal

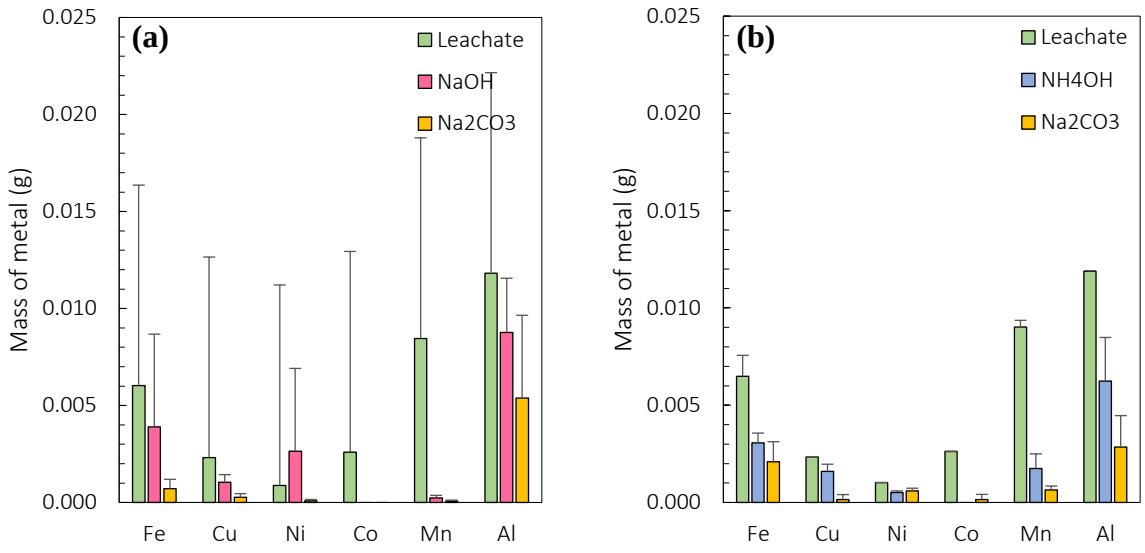

Figure 3.18. Mass of metals in oxalic acid leachate and supernatants after addition of (a) NaOH and (b) NH_4OH and Na_2CO_3.

It was attempted to remove all impurity metals through NaOH and NH_4OH precipitation. From the diagram (Figure 3.18), it can be seen the mass of metals in the initial leachate, after addition of NaOH/ NH_4OH, and after the final addition of Na_2CO_3. The content of lithium in the same solutions is presented in figure 3.20. By the use of NaOH (a) depicted in pink bars, it can be seen an efficient removal of Ni, Co, and Mn, whereas values for Fe, Cu, and Al are considerably higher (removal by 33%, 50%, and 25%). From using NH_4OH (b, blue bars) the removal of Co and Mn are 100% and 77%, respectively. The remaining metals are removed by 50% or less.

The insufficient removal of all metals might be due to the overall low concentrations which complicate the supersaturation (Table A 1 in Appendix A). Although high error bars are depicted, there are not great variations in the mass (the bars look huge due to the low values < 20 mg). However, from the diagram of metal hydroxide solubility (Figure 1.5 in Section 1.5), it can be seen that the solubility of Fe, Al, and Cu increases above a pH of 4 [25, 42]. The theory coincides with the worse removal of these three metals. It might be that the metals precipitate and then dissolves back into the solution as the pH increases above 4. Moreover, ammonia is commonly used as a leaching agent [2]. It is reasonable to believe that soluble ammonia complexes could form, and metals remain dissolved.

It is indicated that a complete Mn recovery cannot be achieved below a pH of 10.6, this might be the reason for its incomplete removal [16]. This is reported for other metals Ni and Co as well [18]. Assuming that a soluble nickel oxalate is present in the solution (Section 3.3.5), it

could be that an intermediate of $M(NH_4)_2C_2O_4$ was formed, and furthermore remained dissolved due to the presence of ammonia, as it formed a soluble metal-ammine complex [43]. Moreover, it might be that the sodium/ammonia reacted with the oxalate and co-precipitated as sodium/ammonia oxalate, due to their low solubility (31.4 g/L and 44.5 g/L) [16].

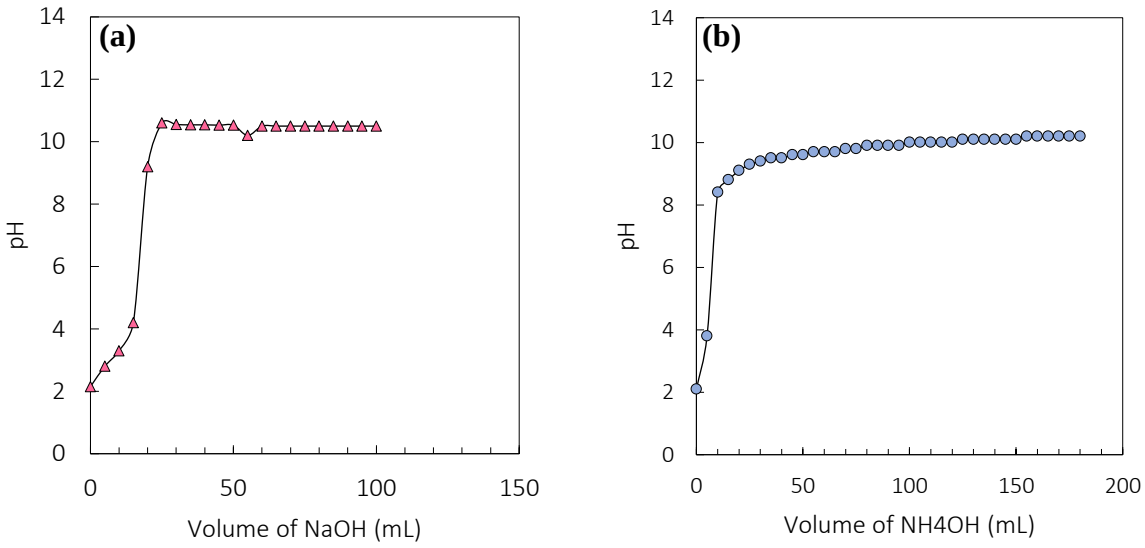

Figure 3.19. pH as a function of volume (a) NaOH and (b) NH_4OH added during precipitation.

The diagrams present pH vs. volume of precipitant. Pink triangles correspond to pH evolution with by addition of NaOH (a), whereas the blue dots (b) show the trend with NH_4OH addition. A similar trend is seen in both diagrams. A slight increase from pH 2- 4, evolves to a steeper rise above pH > 4. When the pH reaches 10. 5 the graph flattens out (a), the corresponding trend is seen with the use of NH_4OH. The flat response in pH despite the increasing volume of precipitant indicates that the precipitation agent is consumed. The lower volume of NaOH required to reach a pH of 10 in (a) (compared to (b)), is due to its stronger alkalinity. The consumption of NaOH/ NH_4OH might be due to the formation of metal hydroxides from the following reaction equation (Section 1.5) [14, 25]:

$$M^{2+} + 2(OH)^{-} \leftrightarrow M(OH)_2 \downarrow \quad (3)$$

The slight trend from pH 2-4 corresponds to possible precipitation of Fe, Al, and Cu hydroxides (Figure 1.5 in Section 1.5). After reaching pH > 10, the trend remains flat. Considered from the same diagram (Figure 1.5), it indicates precipitation of Ni, Mn, and Co.

3.6. Recovery of Lithium from Solution through Crystallization

For the selective recovery of lithium as lithium carbonate, Na_2CO_3 was utilized. The different basis may have affected the precipitation efficiency. Results are presented below.

3.6.1. The Effect of Solution Chemistry on Lithium Precipitation

The attempt to selective lithium recovery as lithium carbonate by (a) sodium carbonate and (b) ammonia, is depicted below (Figure 3.20). Evaporation of the supernatant was done prior to the addition of precipitant [18]. Na_2CO_3 was added to the supernatant solutions in a 1.5 ratio (1:1.5 of Li:Na_2CO_3) [30]. The experiment was conducted at 90˚C due to the low solubility of Li_2CO_3. Concentration of metals in the original leachates can be found in Table X, Appendix A (O-53-70.X).

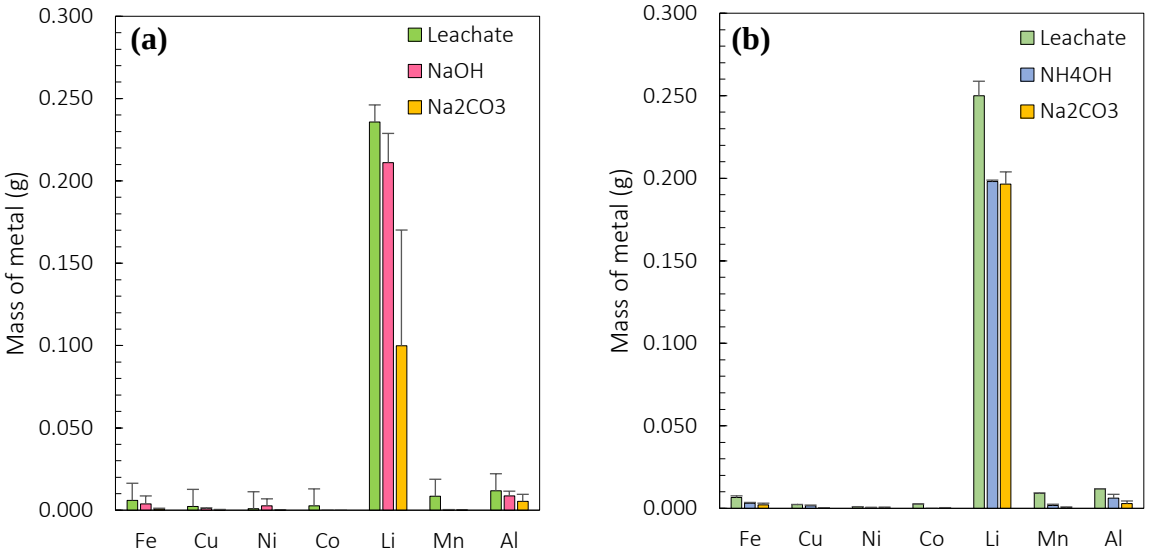

Figure 3.20. Mass of metal in initial leachate, and supernatant solutions after removal of impurities by the use of (a) NaOH and (b) NH_4OH, and selective precipitation of Li using Na_2CO_3.

One of the NaOH experiments was attempted with no evaporation, this resulted in lithium recovery by 16% (0.2203 g to 0.1848 g) (leachate O-53-70.2). However, by subsequent evaporation of this supernatant, the recovery increased by 125% (16-36%). The enhanced result might be due to the increased concentration of Li through evaporation, which in turn induces greater possibilities for supersaturation to occur.

Na_2CO_3 is extensively used as a precipitation agent in the recovery of lithium. Although high efficiencies were not obtained (48-64%) in similar research, it is proven that Li_2CO_3 crystallization can be achieved by increasing the pH above 10 [42]. Zhu et al. increased the pH to 11 to enhance the selective precipitation [30]. The various solution media might also have

affected the precipitation, in terms of e.g., common-ion effect [26]. However, the recovery of lithium as lithium carbonate has some drawbacks. The high solubility at ambient temperatures requires a high temperature for the salt to form insoluble precipitates. Furthermore, the high-temperature requirement imposes a high energy demand [2].

An alternative to selective precipitation could be direct evaporation. Evaporating the $Li_2C_2O_4$ leachate directly would result in solid lithium oxalate. Calcination of this solid precipitate would decompose to Li_2CO_3. However, that would require a considerable amount of energy and thus not be economical [16].

3.6.2. Effect of Molar Ratio on Crystallization of Lithium

In an attempt to increase the recovery of lithium as solid lithium carbonate, various molar ratio of precipitation agent (Na_2CO_3) was added to the supernatant solution.

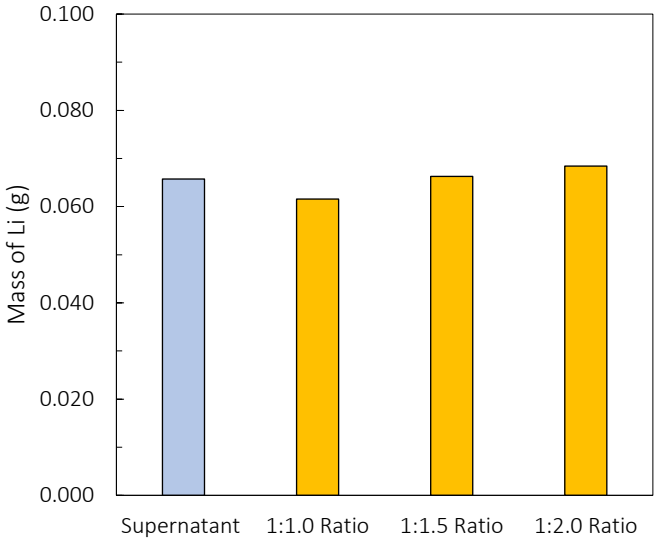

Figure 3.21. Mass of lithium in initial solution (NH_4OH) and supernatants after addition of Na_2CO_3 in different molar ratios.

The figure above is constructed from MP-AES analysis of the initial solution, and subsequent supernatants after addition of precipitation agent in different molar ratios. The y-axis presents the mass of Li in the respective solutions and is calculated from volume (Appendix B). A mass of ≈ 0.07 g of lithium is detected in the initial solution, and the mass remains unchanged in the resulting solutions after precipitation regardless of molar ratio.

From the precipitation experiments using NaOH (Section 3.5), the solutions were evaporated after removal of impurity metals in order to increase the concentration of Li. In these

experiments, evaporation was not performed due to the insolubility of Li2CO3 in ammonia. As the results demonstrated no change in concentration before and the after addition of precipitation agent, evaporation of the same solutions was attempted. The results remained the same (Figure 3.21).

$$Na_2CO_3 + Li_2C_2O_4 \leftrightarrow Li_2CO_3 + Na_2C_2O_4 \quad (4)$$

From the reaction equation (Section 1.5) can be seen a 1:1 ratio between the two components (sodium carbonate and lithium carbonate). Thus, adding the precipitation agent in a 1:1 ratio should be sufficient for the reaction to occur. However, adding excess sodium carbonate will shift the equilibrium to the right (forward direction) and enhance the desired reaction. Additionally, a high concentration of Li would favour/aid the precipitation.

Despite the excess of sodium carbonate added (i.e., 1:1.5 and 1:2 ratio), the salt still did not precipitate. In general, the process of precipitation is determined by the metal ion concentration, solution pH and degree of supersaturation of the precipitant. Moreover, the supersaturation is influenced by solubility product (Ksp), temperature, concentration, ionic activity, and solution chemistry [26].

Unsuccessful precipitation of Li could be due to the high solubility of Li_2CO_3 in aqueous solutions (Table 1.3). The solubility of Li_2CO_3 at 25˚C is 1.28 g/100mL, and apart from most salts, its solubility decreases with increasing temperature [29]. For that reason, a high temperature during the last precipitation was attempted to enhance the Li recovery.

However, the energy barrier for homogeneous nucleation to occur is usually too high to enable precipitation. In the availability of a solid surface, the interfacial free energy (ΔG*) decreases, so does the activation energy barrier for nucleation [26]. Thus, adding solid lithium carbonate to the solution could enhance the precipitation in terms of secondary nucleation i.e., seeding. A high concentration of reactants does not necessarily mean that the free concentration of the relevant ions is equally high in solution. If Li binds strongly to the oxalate, and thereby exhibit a low activity of free Li ions in the solution, this could decrease the supersaturation [26].

3.6.3. Characterization of Precipitate

Characterization of the solid precipitate from selective lithium precipitation is examined through XRD, the result is depicted from this XRD pattern.

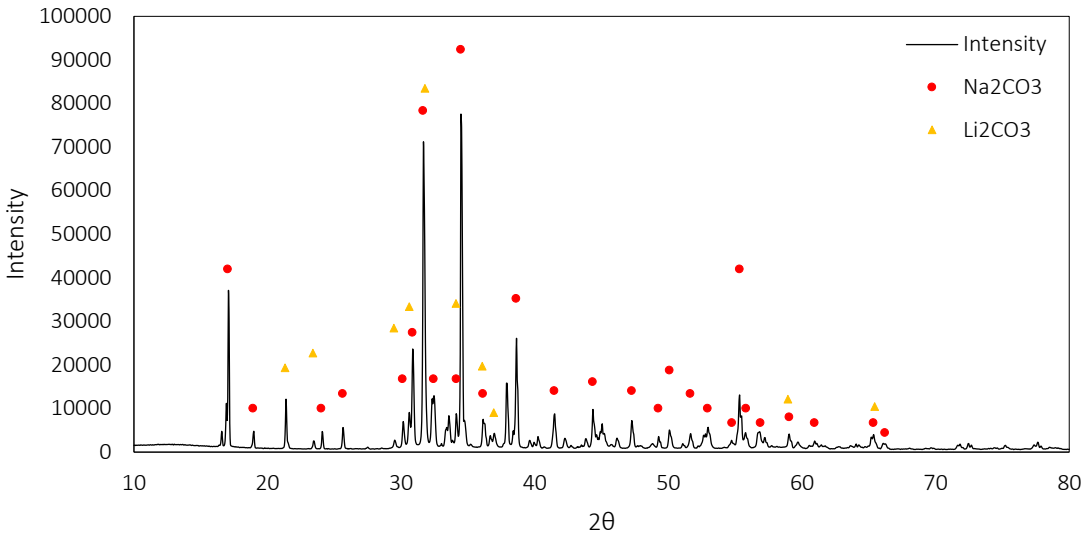

Figure 3.22. XRD pattern of solid precipitate from selective lithium precipitation.

Figure 3.22 presents the XRD pattern of precipitate from selective Li precipitation using Na_2CO_3. The experimental procedure is explained in section 2.7. To ensure sharp peaks and a sufficient number of points per peak, low crystallinity was assumed. The step size and step time is set to 0.050˚ and 3.7, respectively, additional measurement conditions can be found in section 2.2. The range of the 2θ angle was predicted from the database of compounds to be expected [38].

The presence of sodium carbonate can be seen as red dots above high-intensity peaks at 2θ = 17, 31, 35 and 37 (PDF 00-020-1149) [38]. Moreover, Li_2CO_3 is identified and designated as yellow triangles (PDF 00-022-1141) [38]. The pattern indicates that the precipitate consists of both sodium carbonate and the desired lithium carbonate. However, the pattern demonstrates that Li_2CO_3 is detected, and MP-AES confirms a low concentration of Li in the corresponding supernatant (0.003 g/L), this yields a 100% efficiency. The desired precipitation reaction can be expressed by the following reaction equations (Section 1.5):

$$Na_2CO_3 + Li^{2+} \leftrightarrow Li_2CO_3 + Na^{2+} \quad (11)$$

$$Na_2CO_3 + Li_2C_2O_4 \leftrightarrow Li_2CO_3 + Na_2C_2O_4 \quad (4)$$

The initial concentration of Li in the supernatant solution (after removal of impurities, section 3.5) was 1.35 g/L in a total volume of 160 mL. In order to selectively precipitate Li, it was added 44 mL of Na_2CO_3 (1:1.5 ratio) to a total of 200 mL. Evaporation during the precipitation experiment reduced the volume to 60 mL. The reduction corresponds to a 70% decrease, which

in turn should increase the Li concentration by 70%. The higher concentration of Li ensured precipitation of Li_2CO_3, this is confirmed by the XRD pattern.

Lithium carbonate is very soluble, and apart from most salts, its solubility decreases with increasing temperature. The solubility of sodium carbonate increases with increasing temperature. The aqueous solubility of Li_2CO_3 and Na_2CO_3 at 90˚C is 0.78 and 30.9 mg/100mL, respectively (Table 1.3) [29]. The solubility of 0.78 g/100mL at 90˚C, implies that a minimum Li concentration of ≈ 1.5 g/L is required for precipitation to occur, meaning that only minor evaporation was needed in order to obtain a sufficient Li concentration [33]. A high temperature was chosen to aid the precipitation and achieve favourable conditions for supersaturation. However, as the temperature increases and evaporation take place, the solution might become supersaturated with respect to Na_2CO_3 as well, and that could be the reason for co-crystallization [26]. An attempt to wash the precipitate with DI-water may have removed the sodium and increased the impurity of Li_2CO_3 [14].

3.7. Overall Mass Balance of Lithium

In section 2 it is presented an overall flowsheet to the process of selective lithium recovery. As stated in the goals and motivation section, the aim of this work was to selectively recover lithium from lithium-ion batteries of electrical vehicles.

The block flow diagram presents an overall distribution of lithium throughout the process stages and allows for an easy determination of stagewise efficiency (Figure 3.23). The whole experimental part is congregated in an attempt to clarify the entire process. It can be seen how the substantial part of Li is recovered in the selective lithium dissolution by using oxalic acid, whereas the leftovers are collected in the subsequent leaching step (Figure 3.13 in Section 3.3.5). From the two dissolution stages, a total recovery of 80-86% of lithium in solution can be calculated. Furthermore, it is demonstrated that although Li is successfully recovered in solution, the precipitation stage yields poor efficiency and needs to be improved (Section 3.6).

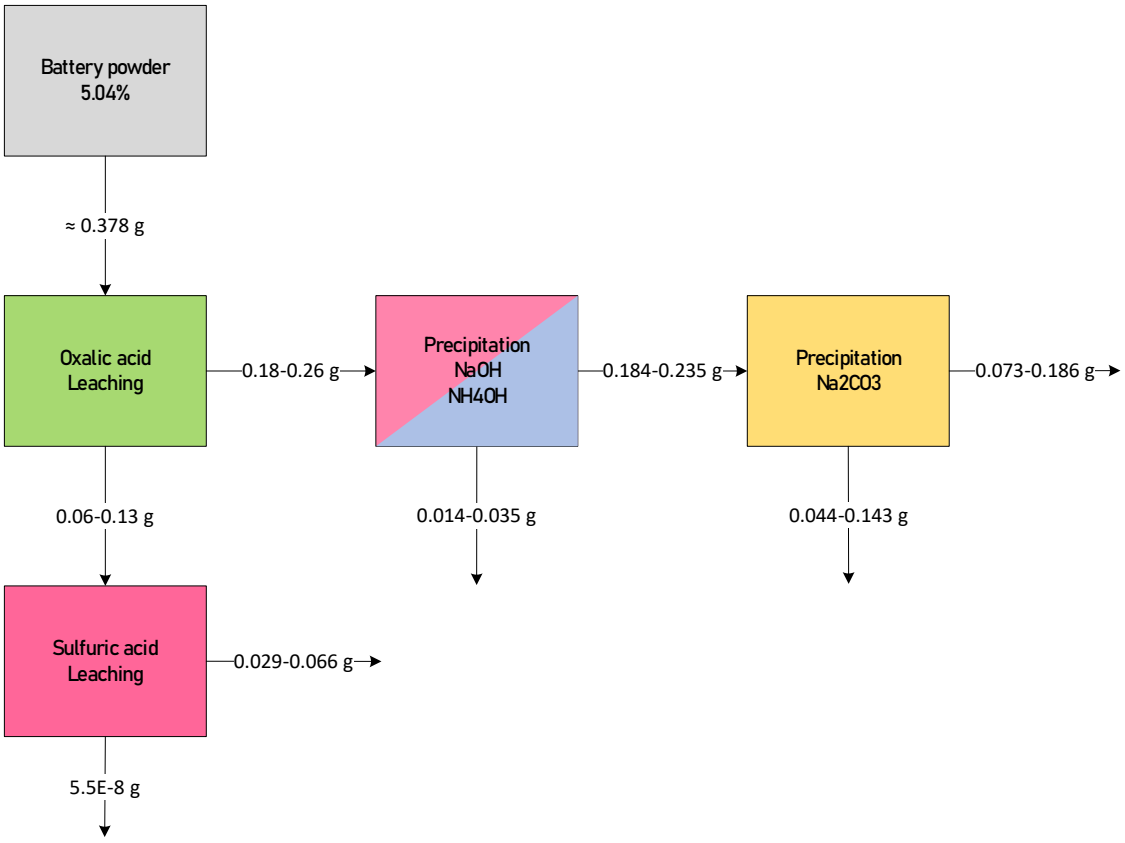

Figure 3.23. Overall mass balance of lithium.

4. Conclusions

As mentioned in the introduction, there are several challenges related to the recycling of LIB electrode materials. In particular the wide variety of different cell chemistries used to compose the anode and cathode. Any one cell type requires slight or moderate adaption to the general approach being used, and this intricates the establishment of a standardized infrastructure.

In an attempt to meet the goals of cost efficiency, high recovery rates and less environmental impact, a hydrometallurgical approach was employed for the recovery of lithium. The recycling will preserve the environment in terms of reduced raw material extraction and appropriate waste management, which will induce energy savings and diminish the emission of harmful materials. The common high-temperature treatment is also eliminated by employing a hydrometallurgical route. This further reduces energy consumption and thus capital costs. Moreover, no metals are lost in a slag, which increases the recovery rates with respect to all metals.

There is a trade-off between costs and recovery rates. Sulfuric acid is cheaper and leaches out all metals in moderate amounts. Reducing agent aided the efficiency and provide efficiencies in the range of 83-100% for the different metals. For the sake of lithium, a selective dissolution was succeeded by oxalic acid. Maximum efficiency of 63% was achieved with an s/l-ratio of 30 g/L and 53˚C, with only a minor co-dissolution of Al. The use of organic acid generates an additional step in order to recover the remaining metals, and as demonstrated in the results, the subsequent inorganic acid leaching yielded lower efficiencies (-83%, -40%, and -16% for Ni, Co, and Mn, respectively) compared to the one of the initial black mass directly. Regarding the recovery of solid lithium in the form of Li_2CO_3, the results obtained was insufficient. Although the presence of Li_2CO_3 was detected by XRD, a considerable amount of Na_2CO_3 is believed to have co-precipitated with it. Thus, an optimization of this stage is necessary.

Although this is lab-scale research and the approach is rather labour intensive, it is desired to automate a portion of the recycling process. In the bigger picture, the limitations of automation narrow down to cell opening and separation of electrode materials, not separation and disassembly of the battery pack components. However, the provided black mass used in this research is a result of shredding the whole battery pack, meaning that it contained materials from both the anode and cathode. Treating it as a whole will contribute to the goal of increased automation. Additionally, it will decrease operational costs.

5. Future Work

As suggestions to optimize the process in terms of higher metal recovery, one could attempt to:

Vary the molar concentration of oxalic acid.

An attempt to increase the lithium dissolution through varying the oxalic acid concentration was not attempted. Although oxalic acid has a high solubility in aqueous solutions (108 g/L) at ambient temperatures (25˚C), the solubility of 108 g/L corresponds to molarity of 1.2M. From the preparation of 1 M solution, difficulties in terms of solubility were experienced. The dissolution was time-consuming, and the suspension had to be shaken vigorously for a longer time to dissolve all the crystals. For that reason, preparation of higher molarity was not attempted. However, a slight increase in molarity is believed not to pose a significant increase in Li dissolution. Li et. al investigated the effect of acid concentration, and it was demonstrated a percentage increase of <1% as the molarity varied from 1.5 M to 2M [16]. Nonetheless, preparing a supersaturated solution by heating could be attempted.

Improve the stage of impurity removal.

From the results, it was observed a poor removal of Al from leachate solutions (Figure 3.18in Section 3.5). A similar trend could be seen for metals Fe and Cu. The low efficiency could be due to the high pH of the solution. A precipitation diagram of metal hydroxides indicates that $Al(OH)_3$ will precipitate in the pH range of 1-6. An increase in pH from a value of 6, shifts the trend and increases the solubility. The diagram demonstrates the same trend for Fe and Cu [25]. Adding an extra filtration step at a pH = 5 could enhance the removal. The updated flow sheet is presented below (Figure 5.1).

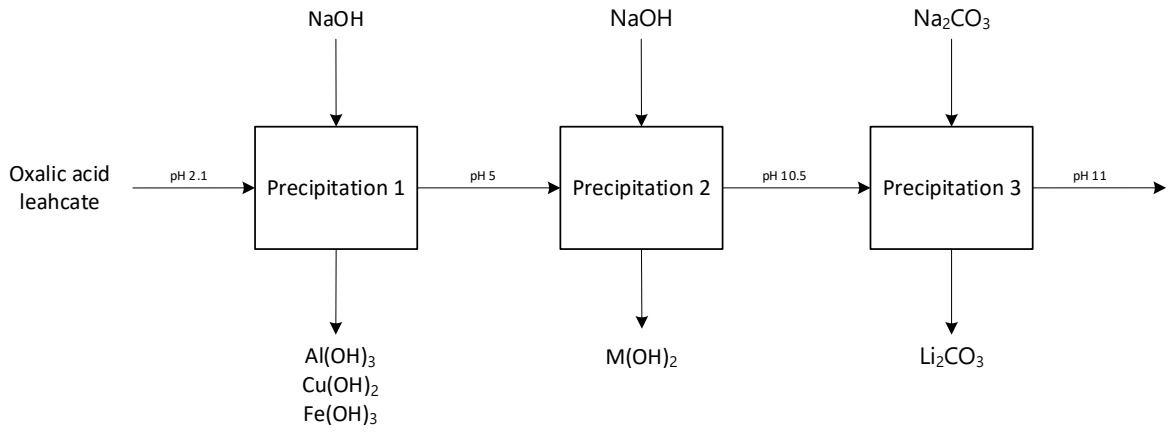

Figure 5.1. stagewise removal of impurities by precipitation.

Moreover, Na_2S could be used to remove Cu in the additional step. Sodium sulphide is preferred as a precipitation agent to recover copper due to the low solubility of CuS in acidic media [22].

Close some loose ends and regenerate the CAM.

Introducing the supernatant solutions after precipitation experiments back into the initial leaching (i.e., feedback loop), might improve the metal recovery thus increase the overall efficiency (Figure 5.2). Adding precipitated metal hydroxides (from the removal of impurities) to the 2.nd leaching (sulfuric acid), allows for dissolution and the metals can be recovered in a four-stage precipitation process [33]. Alternatively, the precipitates could be added directly to the calcination step. Furthermore, recovered Li_2CO_3 could be introduced to the selective li-precipitation in the second route to aid the precipitation by means of increasing the concentration (Section 3.6.2) [26]. Moreover, employing a different precipitation agent, such as KOH or K_2CO_3 might increase the Li recovery [16]. Calcination of the mixed-metal hydroxides (Ni, Mn, and Co) and precipitated lithium carbonate would regenerate the CAM [18]. The resynthesised CAM can be used in new battery production.

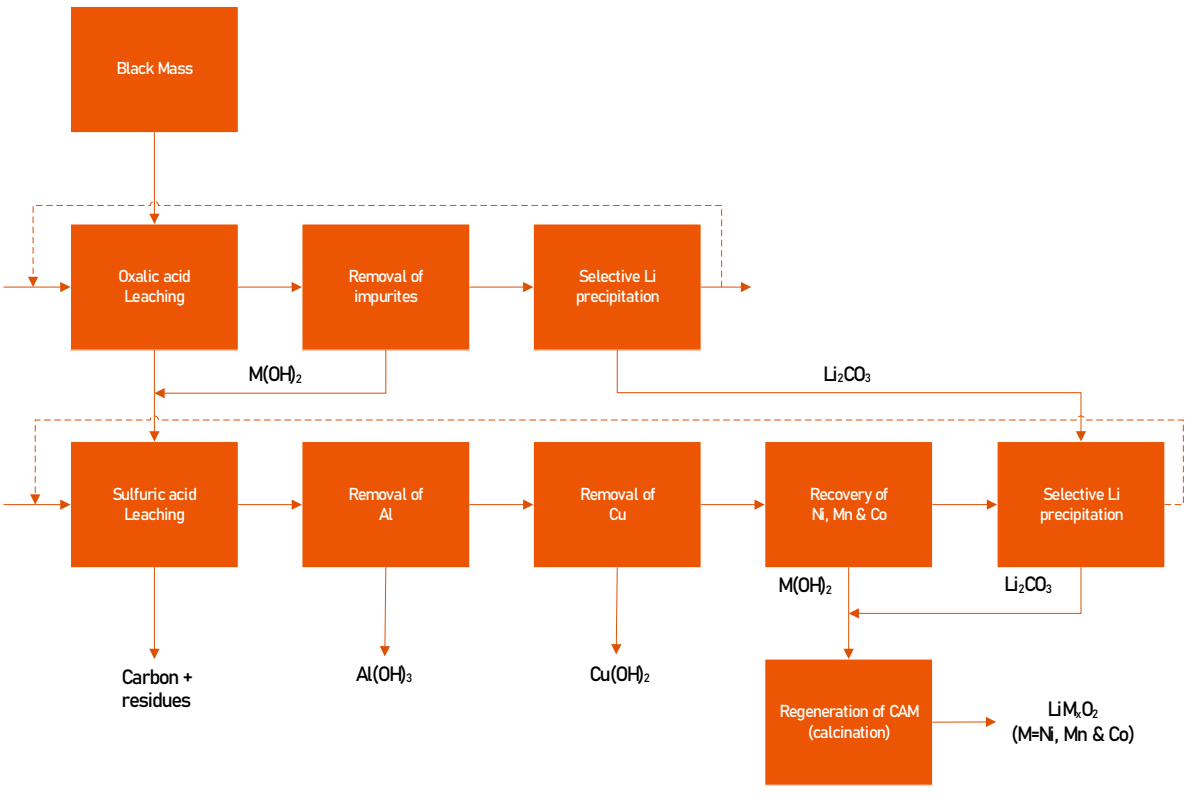

Figure 5.2. Overall flow sheet to the suggested closed loop-recovery.

6. References

1. Or, T., et al., *Recycling of mixed cathode lithium-ion batteries for electric vehicles: Current status and future outlook.* Carbon Energy, 2020. **2**(1): p. 6-43.
2. Yao, Y., et al., *Hydrometallurgical Processes for Recycling Spent Lithium-Ion Batteries: A Critical Review.* ACS Sustainable Chemistry & Engineering, 2018. **6**(11): p. 13611-13627.
3. Storage, C.E., *The lithium-ion battery life cycle report* 2020: London.
4. Kwade, A. and J. Diekmann, *Recycling of Lithium-Ion Batteries The LithoRec Way*. 1st ed. 2018. ed. 2018, Germany: Springer
5. Ryall, N., *How will tomorrows lithium-ion batteries be better than todays?* Catalyst Magazine, 2020(39): p. 4.
6. Wentker, M., M. Greenwood, and J. Leker, *A bottom-up approach to lithium-ion battery cost modeling with a focus on cathode active materials.* Energies, 2019. **12**(3): p. 504.
7. Ma, S., et al., *Temperature effect and thermal impact in lithium-ion batteries: A review.* Progress in Natural Science: Materials International, 2018. **28**(6): p. 653-666.
8. Irle, R. *Global Plug-in Vehicle Sales Reached over 3,2 Million in 2020*. 2021 [cited 2021 06.18]; Available from: https://www.ev-volumes.com/.
9. Beaudet, A., et al., *Key Challenges and Opportunities for Recycling Electric Vehicle Battery Materials.* Sustainability, 2020. **12**(14): p. 5837.
10. Mossali, E., et al., *Lithium-ion batteries towards circular economy: A literature review of opportunities and issues of recycling treatments.* Journal of environmental management, 2020. **264**: p. 110500.
11. Harper, G., et al., *Recycling lithium-ion batteries from electric vehicles.* Nature, 2019. **575**(7781): p. 75-86.
12. Samarukha, I., *Recycling strategies for End-of-Life Li-ion Batteries from Heavy Electric Vehicles*, in *Industrial Engineering and Management*. 2020, KTH: Stockholm. p. 52.
13. Kim, S., et al., *A comprehensive review on the pretreatment process in lithium-ion battery recycling.* Journal of Cleaner Production, 2021: p. 126329.
14. Gao, W., et al., *Lithium carbonate recovery from cathode scrap of spent lithium-ion battery: a closed-loop process.* Environmental science & technology, 2017. **51**(3): p. 1662-1669.
15. Verma, A., et al., *Metal recovery using oxalate chemistry: A technical review.* Industrial & Engineering Chemistry Research, 2019. **58**(34): p. 15381-15393.
16. Li, Q., et al., *Process Synthesis: Selective Recovery of Lithium from Lithium-Ion Battery Cathode Materials.* Industrial & Engineering Chemistry Research, 2019. **58**(8): p. 3118-3130.
17. Sohn, J.-S., et al., *Recovery of Cobalt in Sulfuric Acid Leaching Solution Using Oxalic Acid.* Geosystem Engineering, 2006. **9**(3): p. 81-86.
18. Zhang, X., et al., *Innovative Application of Acid Leaching to Regenerate Li(Ni1/3Co1/3Mn1/3)O2 Cathodes from Spent Lithium-Ion Batteries.* ACS Sustainable Chemistry & Engineering, 2018. **6**(5): p. 5959-5968.
19. Wang, F., et al., *Recovery of cobalt from spent lithium ion batteries using sulphuric acid leaching followed by solid–liquid separation and solvent extraction.* RSC Advances, 2016. **6**(88): p. 85303-85311.

20. Chen, W.-S. and H.-J. Ho, *Recovery of Valuable Metals from Lithium-Ion Batteries NMC Cathode Waste Materials by Hydrometallurgical Methods.* Metals, 2018. **8**(5): p. 321.
21. Sun, L. and K. Qiu, *Organic oxalate as leachant and precipitant for the recovery of valuable metals from spent lithium-ion batteries.* Waste Management, 2012. **32**(8): p. 1575-1582.
22. Kang, J., et al., *Preparation of cobalt oxide from concentrated cathode material of spent lithium ion batteries by hydrometallurgical method.* Advanced Powder Technology, 2010. **21**(2): p. 175-179.
23. Sohn, J.-S., et al., *Comparison of Two Acidic Leaching Processes for Selecting the Effective Recycle Process of Spent Lithium ion Battery.* Geosystem Engineering, 2006. **9**(1): p. 1-6.
24. Meshram, P., B.D. Pandey, and T.R. Mankhand, *Recovery of valuable metals from cathodic active material of spent lithium ion batteries: Leaching and kinetic aspects.* Waste Management, 2015. **45**: p. 306-313.
25. Blais, J.-F., et al., *Metals precipitation from effluents.* Practice Periodical of Hazardous, Toxic, and Radioactive Waste Management, 2008. **12**(3): p. 135-149.
26. Mullin, J.W., *Crystallization*. 4.th ed. 2001: Butterworth-Heinemann.
27. Zhang, X., et al., *Toward sustainable and systematic recycling of spent rechargeable batteries.* Chemical Society Reviews, 2018. **47**(19): p. 7239-7302.
28. Zou, H., et al., *A novel method to recycle mixed cathode materials for lithium ion batteries.* Green Chemistry, 2013. **15**(5): p. 1183-1191.
29. Lide David, R., *CRC handbook of chemistry and physics*. Boca Raton, FL: CRC Press. 2005.
30. Zhu, S.-g., et al., *Recovery of Co and Li from spent lithium-ion batteries by combination method of acid leaching and chemical precipitation.* Transactions of Nonferrous Metals Society of China, 2012. **22**(9): p. 2274-2281.
31. Rosenkilde, C. *Li-ion battery (LIB) Recycling*. [Presentation] 2019 [cited 2021 05/06]; Available from: https://www.standard.no/Global/PDF/Arendalsuka%202019/Sirkul%C3%A6r%20%C3%B8konomi/20190815%20-%20Rosenkilde%20Arendalsuka%20-%20Norsk%20Hydro.pdf.
32. Technologies, A., *MICROWAVE PLASMA ATOMIC EMISSION SPECTROSCOPY (MP-AES)*, in *Application eHandbook*. 2016. p. 166.
33. Sastre, J.P.P., *Resynthesis of Cathode Active Material from Electric Vehicle Battery Waste and Metal Quantification along the Route*, in *Chemical Engineering*. 2021, NTNU: Trondheim. p. 112.
34. Berghof Products, I.G., *User Manual | Version 2.3 | Speedwave Xpert Microwave Digestion System*. 2017, Germany.
35. Products, B., *Application Note XT5 | Microwave Digestion of Molybdenum Oxide*. 2020.
36. Laugen, S., *Separation and Recovery of Cobalt, Copper and Nickel from spent Lithium-Ion batteries*, in *Chemical Engineering*. 2020, NTNU: Trondheim. p. 52.
37. Rigaku. *HIGH-POWER BENCHTOP SEQUENTIAL WDXRF SPECTROMETER*. 2021 [cited 2021 06.18]; Available from: https://www.rigaku.com/products/wdxrf/supermini200.
38. (ICDD), I.C.f.D.D., *Powder Diffraction File PDF-4+ database*. 2012, ICDD.
39. Marshall, J., et al., *Disassembly of Li Ion Cells—Characterization and Safety Considerations of a Recycling Scheme.* Metals, 2020. **10**(6): p. 773.

40. Quinn, A., et al., *Electron Backscatter Diffraction for Investigating Lithium-Ion Electrode Particle Architectures.* Cell Reports Physical Science, 2020.
41. de Vasconcelos, L.S., et al., *Grid indentation analysis of mechanical properties of composite electrodes in Li-ion batteries.* Extreme Mechanics Letters, 2016. **9**: p. 495-502.
42. Wang, H. and B. Friedrich, *Development of a Highly Efficient Hydrometallurgical Recycling Process for Automotive Li–Ion Batteries.* Journal of Sustainable Metallurgy, 2015. **1**(2): p. 168-178.
43. Li, Q., K.Y. Fung, and K.M. Ng, *Separation of Ni, Co, and Mn from Spent LiNi0.5Mn0.3Co0.2O2 Cathode Materials by Ammonia Dissolution.* ACS Sustainable Chemistry & Engineering, 2019. **7**(15): p. 12718-12725.
44. Riffenburgh, R.H., *Chapter 15 - Managing Results of Analysis*, in *Statistics in Medicine (Third Edition)*, R.H. Riffenburgh, Editor. 2012, Academic Press: San Diego. p. 325-343.
45. Royappa, A.T., et al., *Copper(I) oxalate complexes: Synthesis, structures and surprises.* Polyhedron, 2016. **119**: p. 563-574.
46. Majumdar, R., et al., *Secondary catalytic reactions during thermal decomposition of oxalates of zinc, nickel and iron(II).* Thermochimica Acta, 1999. **335**(1): p. 43-53.
47. Rhaman, M.M., et al., *Colourimetric and fluorescent detection of oxalate in water by a new macrocycle-based dinuclear nickel complex: a remarkable red shift of the fluorescence band.* Dalton Transactions, 2014. **43**(12): p. 4618-4621.
48. Yang, Y., et al., *Recovery of iron from red mud by selective leach with oxalic acid.* Hydrometallurgy, 2015. **157**: p. 239-245.
49. Liu, C., et al., *Recycling of spent lithium-ion batteries in view of lithium recovery: A critical review.* Journal of Cleaner Production, 2019. **228**: p. 801-813.
50. Szymczycha-Madeja, A., *Kinetics of Mo, Ni, V and Al leaching from a spent hydrodesulphurization catalyst in a solution containing oxalic acid and hydrogen peroxide.* Journal of Hazardous Materials, 2011. **186**(2): p. 2157-2161.

Appendix A

Concentration of Metals in Leachate Solutions

Concentration of metals in leach liquors analysed by MP-AES is presented in the following tables. The Different leachates are named with regards to leaching conditions, X-XX-XX, e.g., “Oxalic acid–Temp–S/L-ratio”.

Table A 1. Concentration of metals from organic acid leaching (Section 2.5).

Concentration of metals (mg/L)							
No.	**Fe**	**Cu**	**Ni**	**Co**	**Li**	**Mn**	**Al**
O-25-110	63.7	11.3	0.8	10.1	2787.0	156.4	182.3
O-25-70	42.0	6.6	6.1	12.3	1847.3	189.5	107.1
O-25-110	62.5	15.7	75.3	40.1	2534.6	306.0	170.8
O-25-30	44.2	7.8	10.2	0.3	720.3	103.1	45.2
O-25-30	18.8	3.7	18.8	3.3	768.2	122.1	45.4
O-53-30	22.4	30.1	7.8	12.5	1031.1	145.8	53.9
O-53-110	83.7	96.6	713.8	435.5	3660.4	487.6	197.6
O-53-70	49.6	24.7	6.7	32.0	2432.4	85.7	115.0
O-53-70.1	37.9	20.9	0.0	7.4	1700.3	41.4	21.2
O-53-70.2	73.5	19.9	10.1	27.9	2447.7	89.4	127.6
O-53-70.3	56.0	25.1	10.2	27.4	2492.8	91.5	127.5
O-53-70.4	73.7	31.2	8.1	22.3	2444.7	88.7	127.0
O-53-70.5	78.8	24.4	10.5	27.2	2695.7	97.5	124.1
O-53-70.6	56.9	24.6	10.8	27.8	2536.9	91.4	124.6
O-53-70.7	52.8	21.6	8.7	32.8	2620.8	89.2	119.4
O-80-30	30.0	37.1	3.4	18.1	953.9	286.3	59.6
O-80-30	25.6	36.5	4.2	17.5	930.3	227.5	58.2
O-80-110	98.1	250.8	469.7	412.3	3627.9	676.5	93.9
O-80-110	73.3	261.9	449.6	398.5	3593.6	667.2	88.6
O-80-70	55.4	61.7	2.0	11.6	2113.3	204.5	127.2

Results from the inorganic acid leaching is presented in the table below, the naming is based on s/l-ratio and reducing agent, “Sulfuric acid – s/l-ratio – vol% H_2O_2”.

Table A 2. Concentration of metals from inorganic acid leaching (Section 2.4).

Concentration of metals (mg/L)						
No.	**Cu**	**Ni**	**Co**	**Li**	**Mn**	**Al**
S-30-0	215.5	838	751	536	608.5	30.5
O-50-0	377.5	1450.5	1305	933	1062.5	49.5
O-70-0	507	1959	1800.5	1290	1454.5	69
O-90-0	659	2514	2266.5	1589.5	1799.5	88
O-110-0	808	3096	2810	1992	2215	103.5
S-30-3.75	247.5	2067	1910	657.5	1516.5	33
O-50-3.75	414	3521.5	3305.5	1157.5	2630.5	58
O-70-3.75	569.5	4742	4390	1551.5	3507	77
O-90-3.75	676.5	5507	5174.5	1894.5	4181.5	95
O-110-3.75	831	6380	5775	2311.5	4797	114

Appendix B
Calculation of Efficiencies

Calculating Leaching Efficiency

The initial mass of a metal ($m_{M,0}$) was calculated from Aachen analysis (Table 2.2 in Section 2.1) and the mass of powder used in each particular experiment. Results from MP-AES (mg/L) and the volume of leachate (L) was used to calculate the mass of a metal ($m_{M,1}$) in the solution after dissolution. From these two values ($m_{M,0}$ and $m_{M,1}$), the dissolution efficiency (L%) is calculated.

The example below shows the calculation of leaching efficiency with respect to Li from a given experiment:

Table A 3. Experimental data from leaching O-25-110.

Mass of powder (g)	Aachen Li in black mass (wt.%)	MP-AES Experimental conc. of Li (mg/L)	Volume of leachate (L)
7.5018	5.04	2787.0	0.054

Initial mass of Li ($m_{Li,0}$) in ≈ 7.5g black mass:

$$m_{Li,0} = m_p \cdot wt\%$$

$$m_{Li,0} = 7.5018g \cdot 0.0504 = 0.3781g$$

Mass of Li in leachate after dissolution experiment ($m_{Li,1}$):

$$m_{Li,1} = \frac{C_{Li}\,[mg/L]}{1000mg/g} \cdot V_{leachate}[L]$$

$$m_{Li,1} = \frac{2787mg/L}{1000mg/g} \cdot 0.054L = 0.1505g$$

Leaching efficiency with respect to Li:

$$L\%_{\,Li} = \frac{m_{Li,1}}{m_{Li,0}} \cdot 100\%$$

$$L\%_{\,Li} = \frac{0.1505g}{0.3781g} \cdot 100\% = 40\%$$

I.e., 40% of Li in the black mass was dissolved into solution through acid leaching.

Calculating Leaching Efficiency for 2.nd. Leaching

To calculate the efficiency of the second (sulfuric acid) (Section 3.3.5) leaching, the mass of metals in the filter residue from the first leaching was used. The solid residue was digested with the use of aqua regia and analysed by MP-AES to determine the content (wt.%) of metals. The wt.% of metals in the filter cake can be calculated in two ways (mass-wise and from concentration).

Mass of Li in the solid residue ($m_{Li,2}$) used for each particular experiment and in the solution after second leaching ($m_{Li,3}$) was used to calculate the efficiency.

wt.% of metal in solid samples after 1.st leaching:

Table A 4. Experimental data of digested solid residue from organic acid leaching (O-53-30).

Total mass of solid residue (g)	Sample: Mass of solid residue (g)	Sample: Volume of aqua regia (L)	s/l-ratio (g/L)	MP-AES Experimental conc. of Li (mg/L) in digested sample	Volume of digested sample (L)
9.9481	0.0839	0.008	10.5	65.4	0.00625

Based on mass

Mass of Li ($m_{Li,digest}$) in digested sample (containing 80 mg of solid residue):

$$m_{Li,digest} = \frac{65.4 mg/L}{1000 mg/g} \cdot 0.00625 L = 0.0004 g$$

$$wt\% = \frac{m_{Li,digest}}{m_{residue}} \cdot 100\%$$

$$wt\% = \frac{0.004 g}{0.0887 g} \cdot 100\% = 0.49\%$$

Based on concentration

$$wt\% = \frac{C_{Li}\,[mg/L] \cdot 0.001 g/mg}{\frac{m_{sample}}{V_{AquaRegia}}[g/L]} \cdot 100\%$$

$$wt\% = \frac{65.4 mg/L \cdot 0.001 g/mg}{10.5 g/L} \cdot 100\% = 0.62\%$$

To calculate the mass of Li in the whole cake, wt.% is multiplied with the total mass (≈9.94g).

Mass of Li in solid residue used for 2.nd.

To ensure a similar procedure, also for these experiments ≈7.5 g of solid sample was weighed out. This means that only a fraction of whole filter cake is used for the second leaching. To be able to calculate the correct efficiency we need to take that fraction (≈7.5g) into consideration and not the whole cake (≈ 9.9g).

Table A 5. Experimental data from inorganic acid leaching of solid residue (from O-53-30).

Mass of solid residue used for 2.nd. leaching (g)	Li in solid residue (wt.%)	MP-AES Experimental conc. of Li (mg/L) in 2.nd. leachate	Volume of 2.nd. leachate (L)
7.5020	0.49	639.69	0.045

Mass of Li ($m_{Li,2}$) in ≈7.5g of solid residue:

$$m_{Li,2} = m_{sample} \cdot wt\%$$

$$m_{Li,2} = 7.5020g \cdot 0.0049 = 0.037g$$

Mass of Li in 2.nd. leachate and Efficiency

Mass of Li ($m_{Li,3}$) in leachate after 2.nd. dissolution experiment:

$$m_{Li,3} = \frac{C_{Li}\ [mg/L]}{1000mg/g} \cdot V_{2.nd\ leachate}[L]$$

$$m_{Li,3} = \frac{639.69mg/L}{1000mg/g} \cdot 0.045L = 0.029g$$

Leaching efficiency for 2.nd. dissolution with respect to Li:

$$L\%_{\ Li} = \frac{m_{Li,3}}{m_{Li,2}} \cdot 100\%$$

$$L\%_{\ Li} = \frac{0.029g}{0.037g} \cdot 100\% = 80\%$$

I.e., 80% of Li in the filter residue from the first leaching was dissolved through the second leaching.

Calculating Leaching Efficiency for Precipitation Experiments

The efficiency of leaching experiments was calculated from the initial leachate and subsequent supernatant. Mass of metal in the solution is calculated as explained above.

Table A 6. Raw data from precipitation experiment of leachate O-53-70.7.

MP-AES Experimental conc. of Li (mg/L) in leachate	Volume of leachate (L)	MP-AES Experimental conc. of Li (mg/L) in supernatant	Volume of supernatant (L)
2621	0.095	4218	0.044

Mass of Li in leachate after dissolution experiment ($m_{Li,1}$):

$$m_{Li,1} = \frac{C_{Li}\,[mg/L]}{1000 mg/g} \cdot V_{leachate}[L]$$

$$m_{Li,1} = \frac{2621 mg/L}{1000 mg/g} \cdot 0.095 L = 0.2490 g$$

Mass of Li in supernatant after precipitation experiment ($m_{Li,4}$):

$$m_{Li,4} = \frac{C_{Li}\,[mg/L]}{1000 mg/g} \cdot V_{supernatant}[L]$$

$$m_{Li,4} = \frac{4218 mg/L}{1000 mg/g} \cdot 0.044 L = 0.1856 g$$

Precipitation efficiency with respect to Li:

$$P\%_{\,Li} = \frac{m_{Li,1} - m_{Li,4}}{m_{Li,1}} \cdot 100\%$$

$$P\%_{\,Li} = \frac{0.2490 g - 0.1865 g}{0.2490 g} \cdot 100\% = 25\%$$

I.e., 25% of Li was recovered (or removed from the leachate) through precipitation. To calculate the removal of impurity metals

Appendix C

External Calibration curves from MP-AES Software

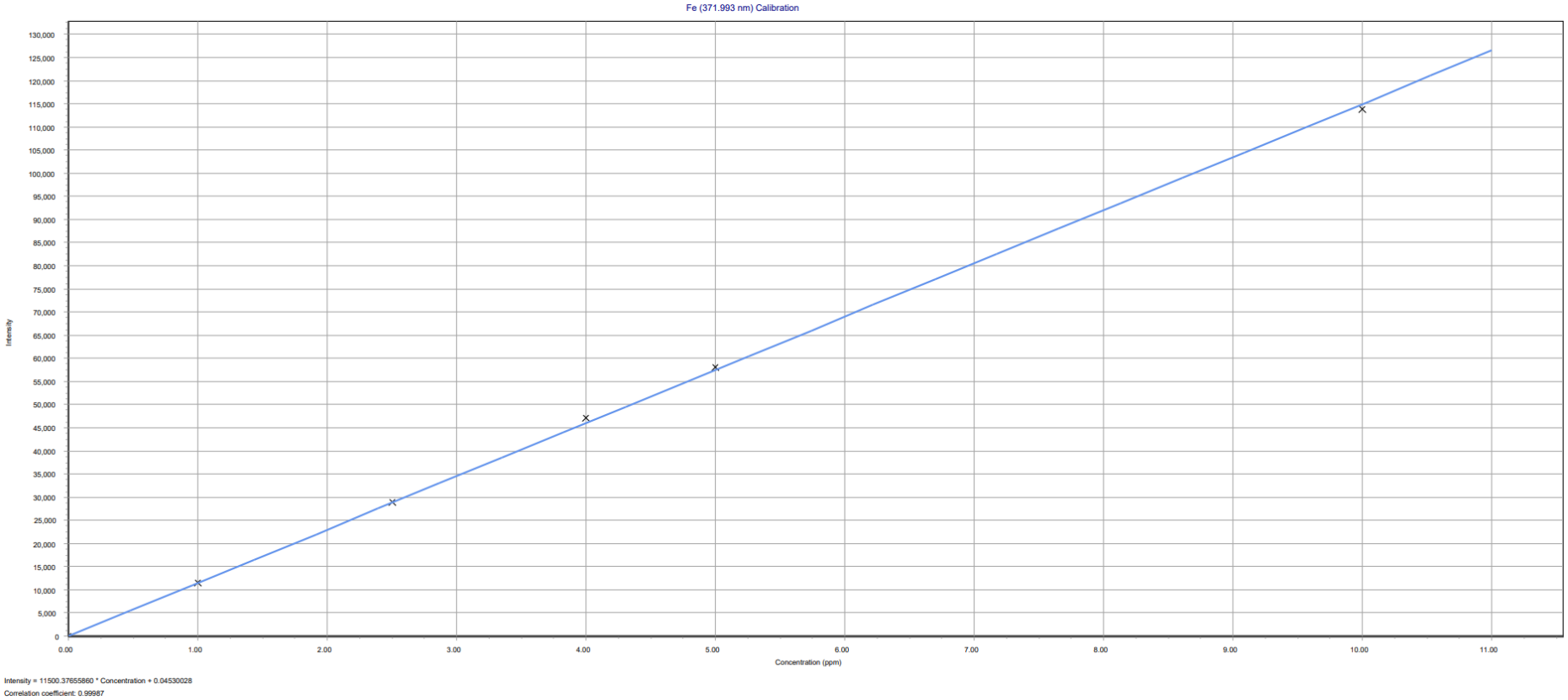

Figure A 1. Calibration curve of iron (372 nm) from MP-AES software.

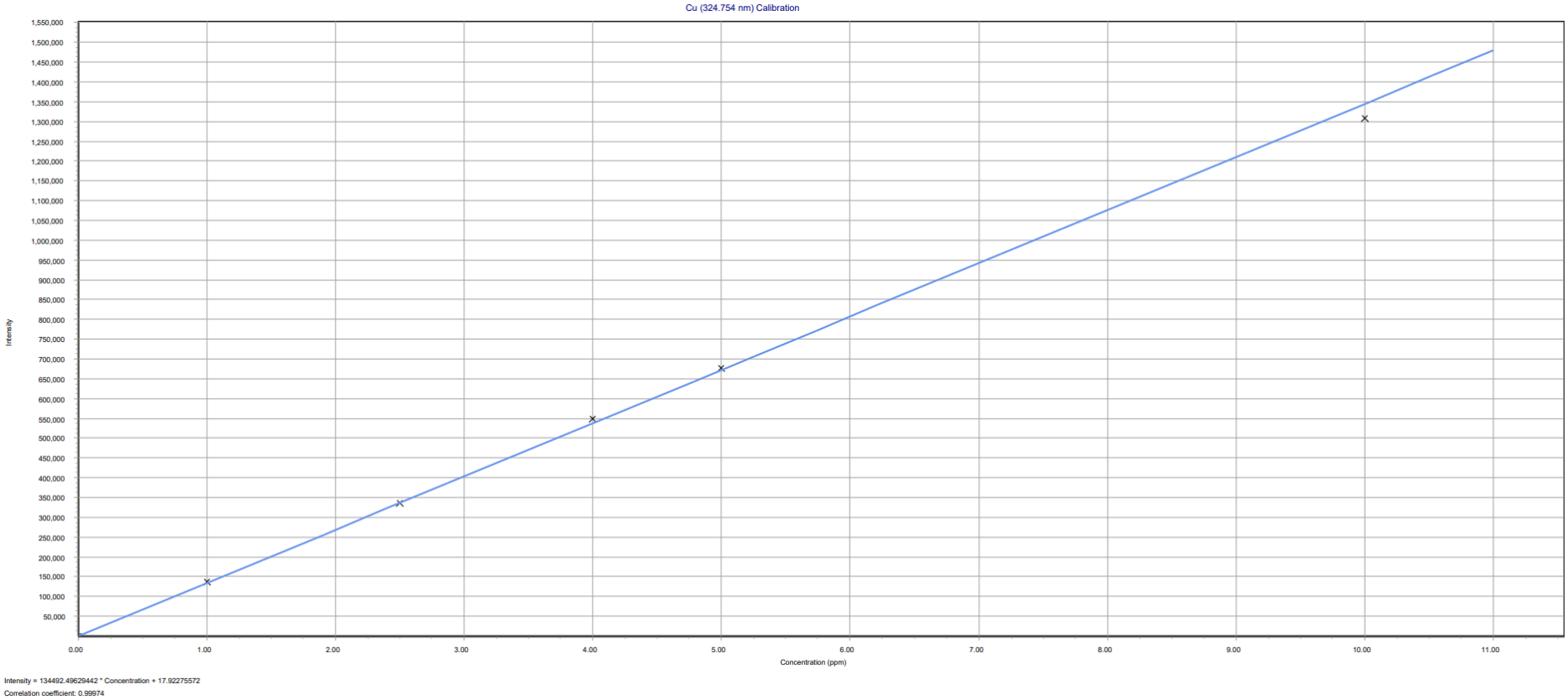

Figure A 2. Calibration curve of copper (325 nm) from MP-AES software.

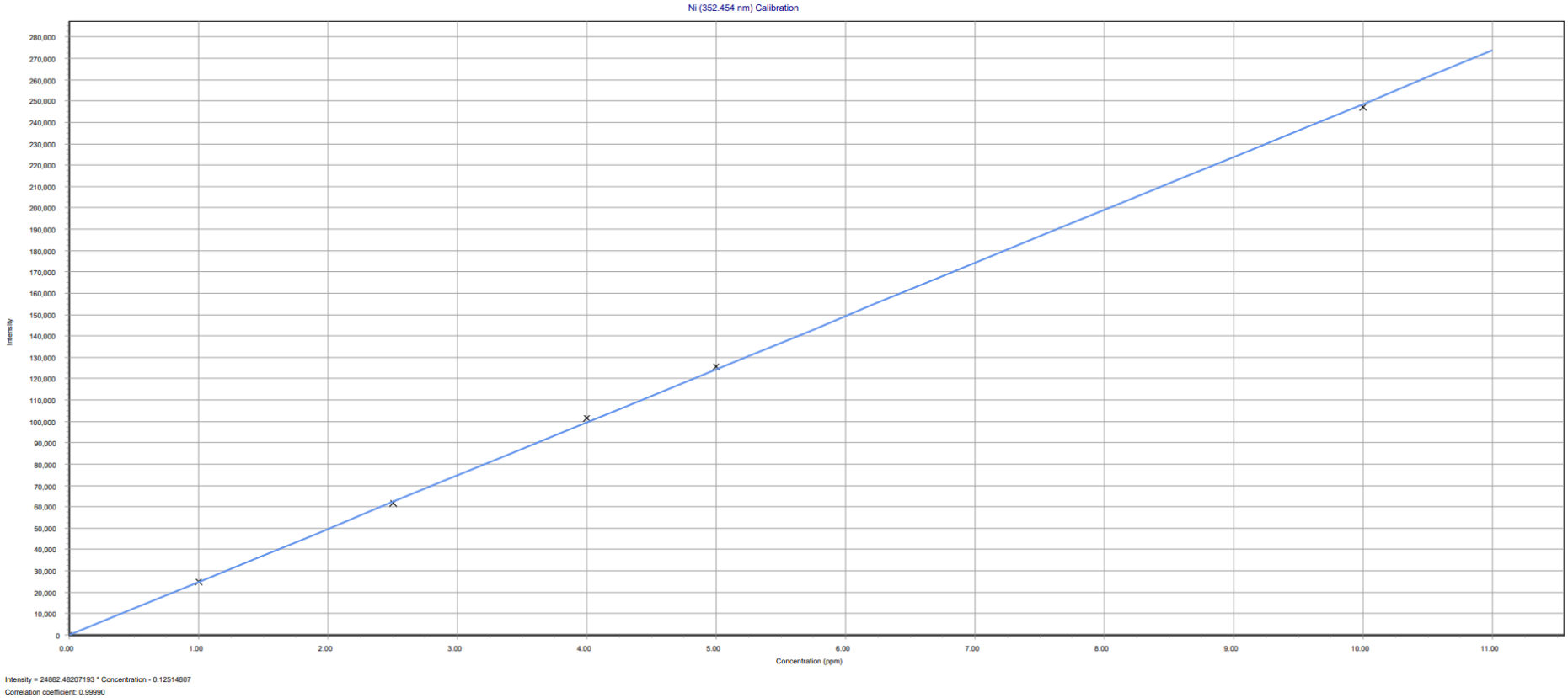

Figure A 3. Calibration curve of nickel (352 nm) from MP-AES software.

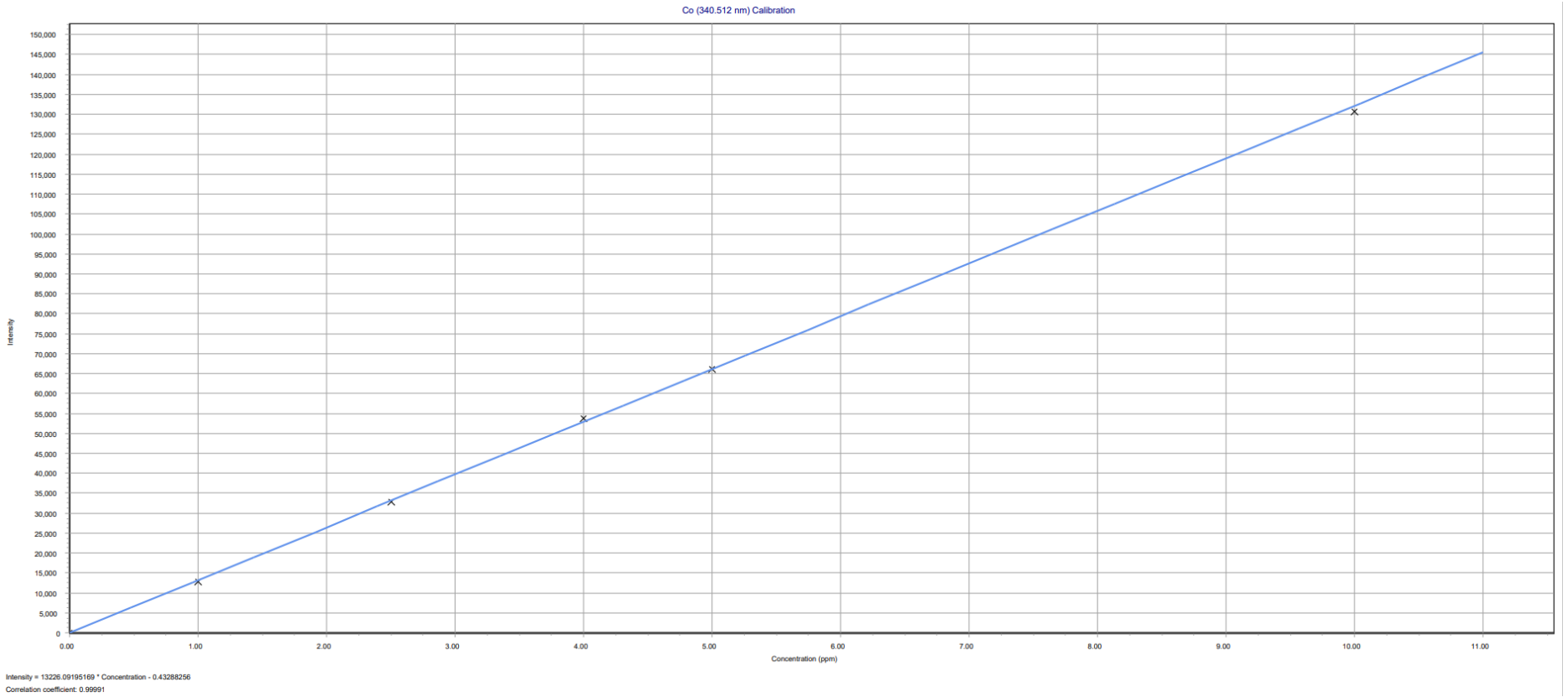

Figure A 4. Calibration curve of cobalt (341 nm) from MP-AES software.

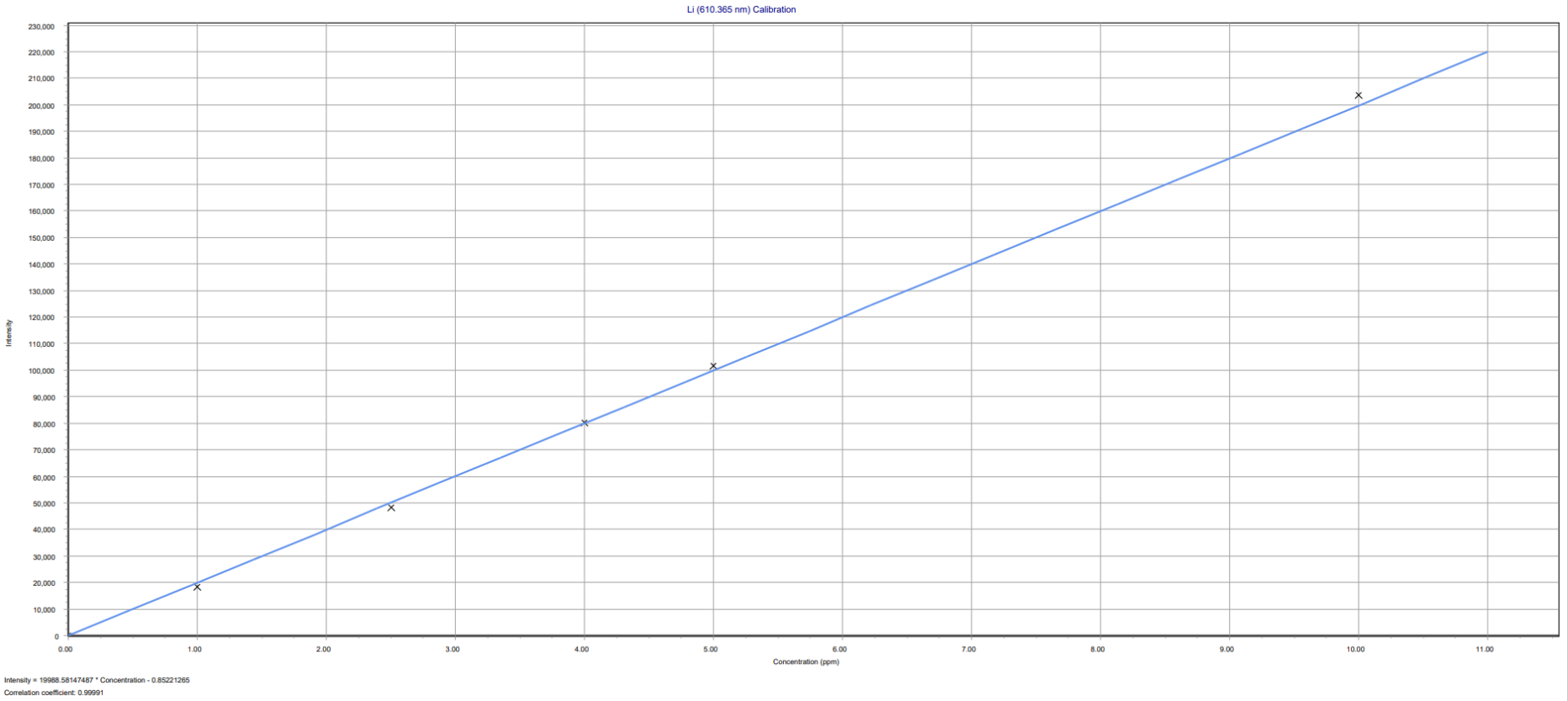

Figure A 5. Calibration curve of lithium (610 nm) from MP-AES software.

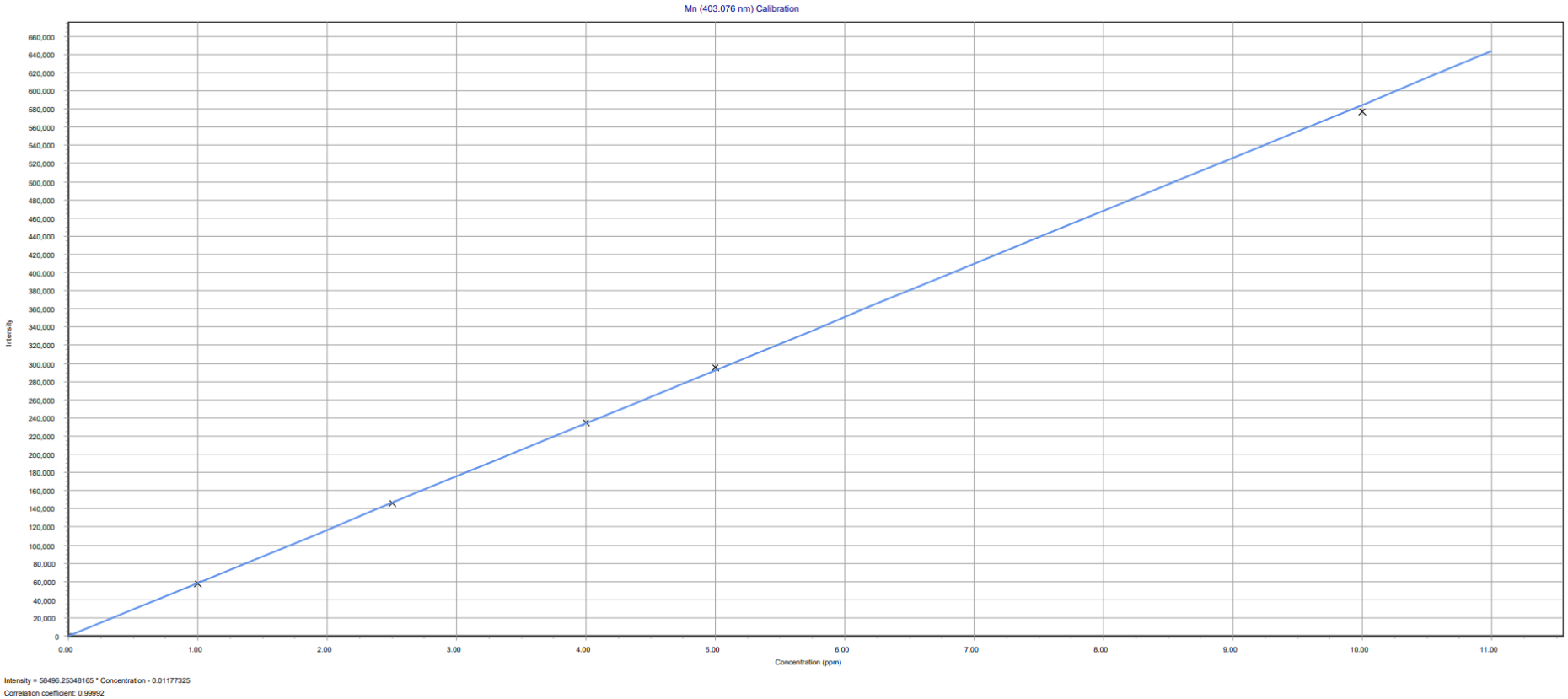

Figure A 6. Calibration curve of manganese (403 nm) from MP-AES software.

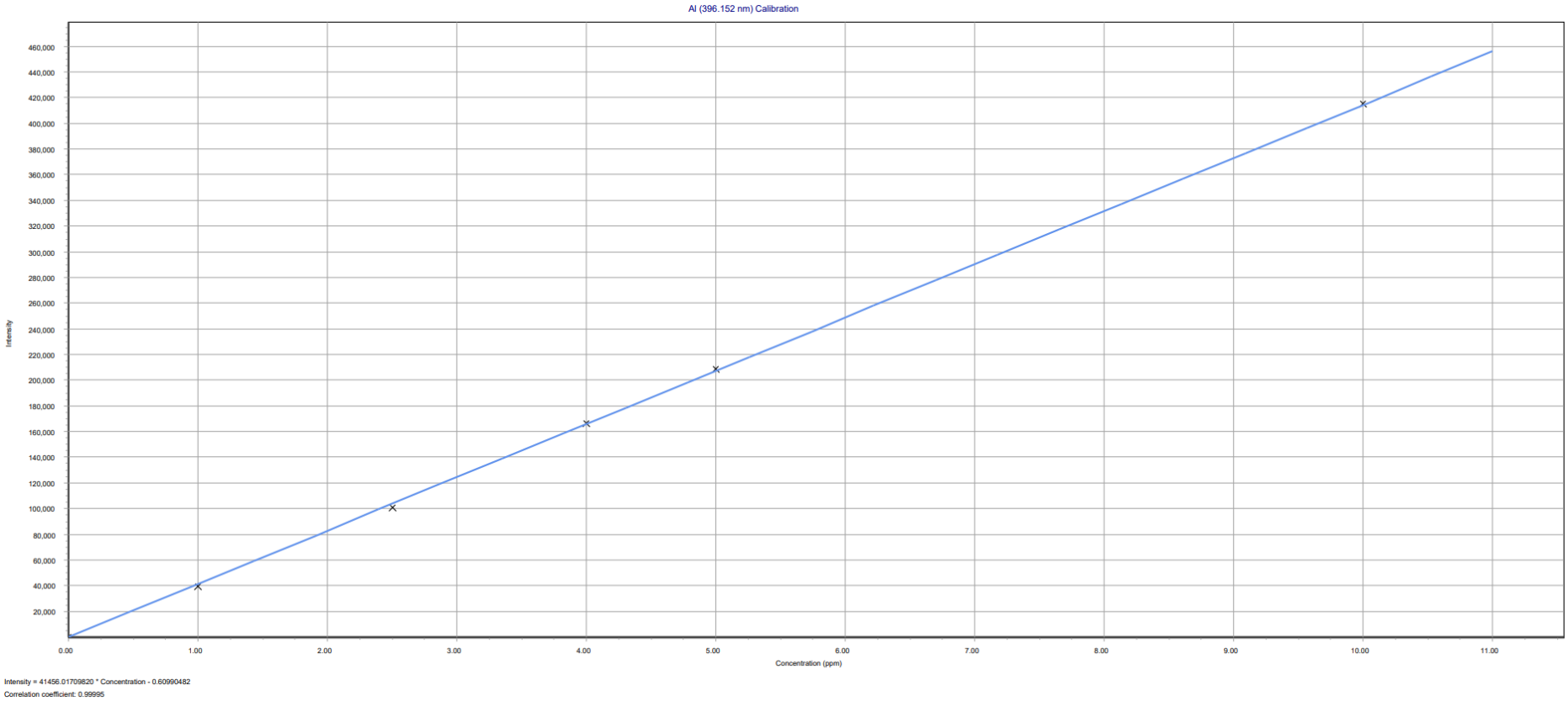

Figure A 7. Calibration curve of aluminium (396 nm) from MP-AES software.

Appendix D

All Excel sheets and calculations can be found in my SharePoint folder. Only people within the NTNU organisation are able to access/open the URLs.

The whole folder of experimental work

https://studntnu.sharepoint.com/:f:/s/o365_HydrometallurgyResearchGroup-StinaSpecializationProjectFall2020/Eh0YA4X_sOpJgKaYyfwe59kB-HttTlsNa6EgF6nNuBzyug?e=v04S4Y

Sulfuric acid leaching:

https://studntnu.sharepoint.com/:x:/s/o365_HydrometallurgyResearchGroup-StinaSpecializationProjectFall2020/EZ975bqv2c5PkHiT11ALPgMBtLiVywrCV2frtl5Pn93mMw?e=9TFmKz

Oxalic acid leaching:

https://studntnu.sharepoint.com/:x:/s/o365_HydrometallurgyResearchGroup-StinaSpecializationProjectFall2020/EajXxXZ7hzJIrSbQj15yM3YB8qt5g2HjS3-GicB7_URHxw?e=Ztbh2c

Digestion of solid samples (black mass and filter cakes):

https://studntnu.sharepoint.com/:x:/s/o365_HydrometallurgyResearchGroup-StinaSpecializationProjectFall2020/EfMnhmv2g75JpmJkG-0Z_D8Buiveh-W7Anth5J92HwW0pQ?e=VSevqP

https://studntnu.sharepoint.com/:x:/s/o365_HydrometallurgyResearchGroup-StinaSpecializationProjectFall2020/ESMTEMcbjMtBmLTQFngHIuMB0UJD-dsNlHrr1tQ0x_H_eQ?e=sQV2VS

Precipitation Experiments:

https://studntnu.sharepoint.com/:x:/s/o365_HydrometallurgyResearchGroup-StinaSpecializationProjectFall2020/Ecqn7Rc6Oq9Mnwh1vXNf2nYBiPJ8e4tZIaNgjWzP_5RtGw?e=jxiBIq

Data from XRD are collected in separate Excel sheets for each separate sample (due to the amount of data), raw data can be found in my folder (IKP>Stina) on the Odin server (all samples are named accordingly to associated Excel sheets). Moreover, all data from MP-AES and XRF analysis can be found in my folder [36] in the respective software/ associated computers.

Background theory for leaching and precipitation can be found in the specialization project:

https://studntnu.sharepoint.com/:b:/s/o365_HydrometallurgyResearchGroup-StinaSpecializationProjectFall2020/EVXFKrtkSCxDhCG7yTC3ga8Bj2taFtr5k-8wHRlyiMoWDg?e=5VCQne

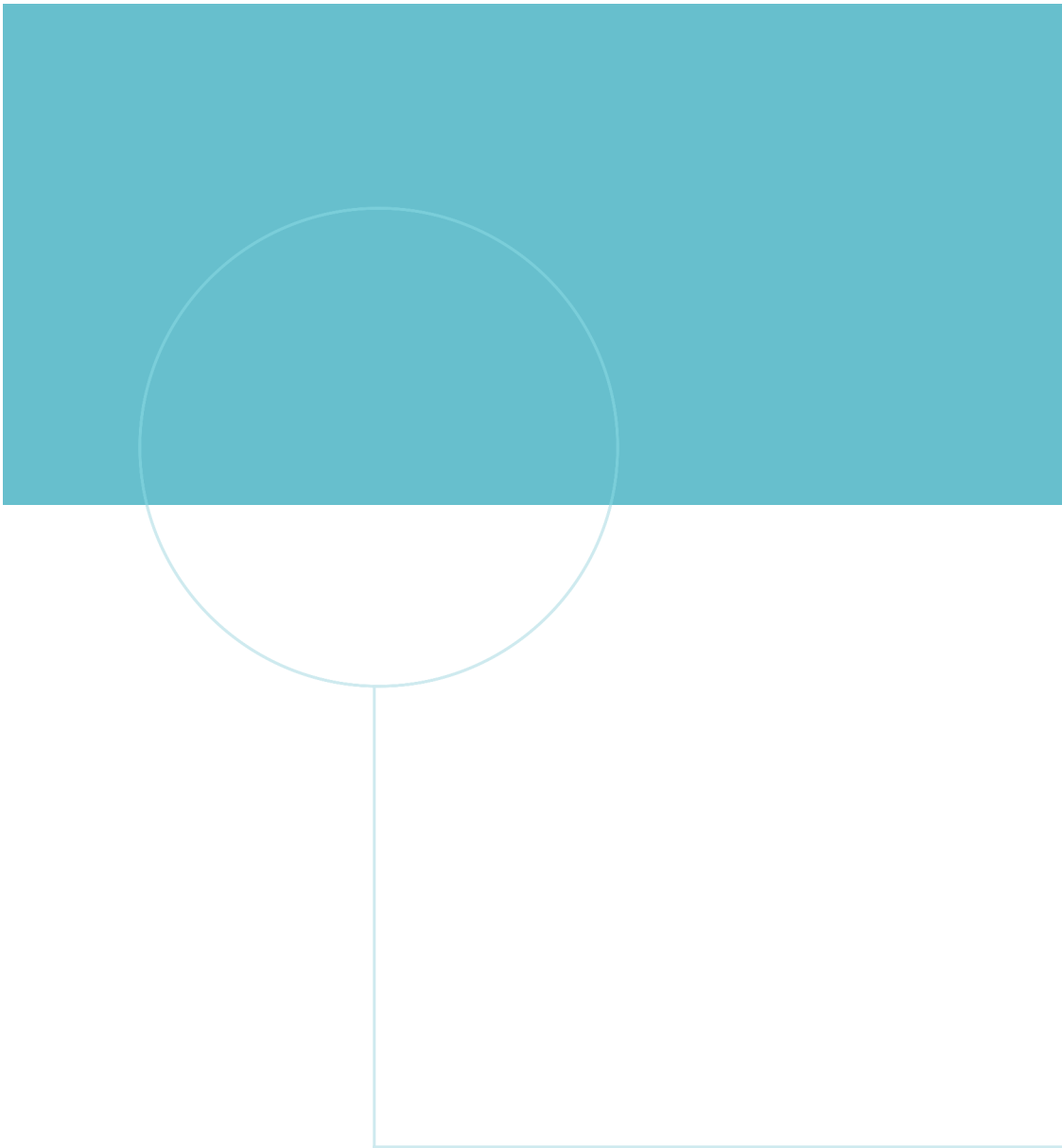

NTNU

Norwegian University of
Science and Technology